Investigation of Solvent Effects on the Hydrodeoxygenation of Guaiacol over Ru Catalysts

Journal:	*Catalysis Science & Technology*
Manuscript ID	CY-ART-09-2019-001763.R1
Article Type:	Paper
Date Submitted by the Author:	01-Oct-2019
Complete List of Authors:	Saleheen, Mohammad; University of South Carolina, Chemical Engineering; Mr. Verma, Anand; University of South Carolina, Chemical Engineering Mamun, Osman; Stanford University Lu, Jianmin; Dalian Institute of Chemical Physics, Chinese Academy of Sciences, Heyden, Andreas; University of South Carolina, Chemical Engineering

Investigation of Solvent Effects on the Hydrodeoxygenation of Guaiacol over Ru Catalysts

Mohammad Saleheen[1], Anand Mohan Verma[1,2], Osman Mamun[3], Jianmin Lu[4], and Andreas Heyden*[1]

[1]*Department of Chemical Engineering, University of South Carolina, 301 Main Street, Columbia, South Carolina 29208, USA*

[2]*Department of Chemical Engineering, Indian Institute of Technology Guwahati, Assam 781039, India*

[3]*Department of Chemical Engineering, Stanford University, Stanford, California 94305, USA*

[4]*State Key Laboratory of Catalysis, Dalian National Laboratory for Clean Energy, Dalian Institute of Chemical Physics, Chinese Academy of Sciences, Dalian 116023, People's Republic of China*

*Corresponding author email: heyden@cec.sc.edu

Abstract

The effects of a liquid phase environment on the hydrodeoxygenation of guaiacol, a prototypical lignin derived compound, have been investigated over a Ru catalyst from first principles. A microkinetic reactor model with parameters obtained from density functional theory and implicit solvation schemes was developed to study the effects of condensed phases on the reaction mechanism and kinetic parameters. Phenol was found to be the major aromatic product across all reaction environments. Our model predicts that less protic solvents such as 1-butanol, diethyl ether, and n-hexane have a positive effect on the reaction kinetics for the production of phenolics relative to vapor and aqueous reaction environments. The dominant reaction mechanism for aromatics production remains unchanged across all reaction media. Next, we investigated the possibility of cycloalkane production through hydrogenation of phenol in vapor and liquid phase environments. Our calculations indicated that the reaction pathway for cycloalkane production from phenol will most likely follow an initial dehydrogenation of the hydroxyl group. Based on the vapor phase density functional theory calculations, we proposed a probable reaction pathway and calculated the condensed phase effects along this reaction route. We observed that an aqueous phase has a more favorable effect for cycloalkane production from phenol relative to vapor phase and other less protic solvent environments.

Keywords: Solvent effects; Guaiacol; Phenol; Hydrodeoxygenation; Microkinetic modeling; Density functional theory; Ruthenium

1. Introduction

The discourse about the feasibility and the economic viability of utilizing biomass as an alternative energy source to produce biofuels has intensified lately.[1] Despite the sustainability and the environmental friendliness of this renewable resource, the over reliance of the existing technologies on food grade biomass resources poses some significant challenges.[2-3] Therefore, upgrading of lignocellulosic biomass to second generation liquid transportation fuels has been receiving widespread attention.[4-6] Thermochemical conversion processes such as flash pyrolysis or hydrothermal liquefaction can be employed to produce environmentally benign bio-oils from these biomass sources. Bio-oils have higher energy density and better transportability than feedstock biomass and can generate CO_2 and SO_x credits with lower NO_x emissions compared to fossil fuels.[7] Dependent on the biomass sources and the conversion processes adopted, the oxygen content in bio-oils can approach as high as 50%, despite having low sulfur and nitrogen content in comparison to fossil-based oils.[8-9] The presence of a large oxygen content combined with corrosive acids and reactive aldehydes in the complex bio-oil mixture leads to several undesirable properties, such as low heating value, high viscosity, non-volatility, thermal instability, high degree of corrosiveness, and tendency to polymerize upon exposure to air[9] which limits the prospect of direct substitution of bio-oils for petroleum fuels. Therefore, some upgrading processes need to be employed to reduce the O/C ratio of the pyrolysis oil for wider range of applications.

Catalytic flash pyrolysis and hydrodeoxygenation (HDO) are two of the most promising catalytic upgrading processes for bio-oil. *In-situ* catalytic flash pyrolysis processes have the advantage of being operated at atmospheric pressure in absence of hydrogen;[7] however, the high degree of oxygen removal and the ability to prevent coke deposition on the catalyst surface have made HDO the more promising alternative.[10] Catalytic HDO of bio-oils is typically performed at high hydrogen pressure to reduce the oxygen content as well as to increase the H/C ratio. Sulfided catalysts such as CoMo and NiMo on γ-Al_2O_3 support have been thoroughly studied for HDO due to their conventional industrial application in the hydrodesulfurization (HDS) of petroleum oils.[11-13] However, the instability of the sulfided catalysts in presence of sulfur free bio-oils,[14-15] evolution of sulfur containing HDO intermediates owing to the co-feeding of H_2S to maintain the sulfide structure,[16] boehmite formation of the acidic support in presence of water present in the bio-oil mixture,[15,17] and deactivation of the catalyst surface by polymerization and coke formation[18-19] restrict the prospect employing conventional HDS catalysts for HDO purposes. The tendency of bio-oils to thermal degradation and coke formation makes noble metals industrially attractive catalysts despite the higher cost due to their excellent activity, selectivity and stability.[16,20] They are expected to operate at mild reaction conditions without any introduction of sulfur, and fast deactivation by coke formation in the presence of phenolic compounds can be avoided by employing a high hydrogen pressure during HDO. Nonetheless, further improvement of the catalyst design by tailoring the active phase and the support is required to reduce the hydrogen consumption and increase the yield of selective oils.

Bio-oils derived from different feedstocks are typically a complex mixture of water (10-30%) and 300 different organic compounds, comprising of insoluble pyrolytic lignin, aldehydes, organic acids, sugar oligomers, alcohols, and phenol derivatives.[21] Guaiacyl species, being the primary structure of lignin, are predominant in bio-oils and tend to repolymerize to form coke and heavy hydrocarbons during bio-oil upgrading processes.[22-23] The presence of these diverse organic compounds complicates the bio-oil upgrading process which makes the mechanistic investigation of reaction pathways and catalytic activities very challenging. Therefore, for better understanding of the catalytic upgrading process, it is imperative to select a model compound representative of the pyrolysis oil. In the current study, guaiacol (2-methoxyphenol) has been chosen as the prototypical compound of phenol derivatives and lignin derived oligomers which contains a phenyl ring, two different oxygenated functions, and has been known to play a significant role in the catalyst deactivation process. HDO of guaiacol over a wide range of monometallic transition metals such as Pt[16,24-31], Rh[16,26,30,32], Pd[16,26,28,30,33-34], Ru[26,28,30,33,35-36], Fe[28,37], Mo[33], Ir[33], W[33], Cu[28,33]; post transition metals such as Sn[24] as well as bimetallic catalysts such as Rh-Pd[32], Rh-Pt[32], Pt-Sn[24], Ni-Cu[38], Pd-Fe[28] have been reported. Due to the critical role of metal-support interaction, support acidity, susceptibility of conventional γ-Al_2O_3 support to coke formation[8,39], and its instability in presence of water[17,39]; various supports such as C[26,28,33,35], ZrO_2[16,32,38], TiO_2[29,35], SiO_2[26,35,37-38], CeO_2[38,40], MgO[27,36] have also been tested rigorously. Heeres et al.[41] presented a thorough catalyst screening using noble metals catalysts and compared that with the conventional hydrotreatment catalysts for HDO of fast pyrolysis oil. They addressed Ru/C as the most promising candidate for bio-oil upgrading regarding oil yields, deoxygenation activity, and hydrogen consumption. Our group has previously reported an in-depth vapor phase mechanistic investigation of the HDO of guaiacol over a Ru(0001) model surface and concluded phenol to be the major product.[42] However, the presence of a substantial amount of water in bio-oil feeds (30%) combined with the production of more water during the HDO process can affect the activity as well as the surface structure and chemical composition of the catalysts.[9] If used as a solvent, water has the potential to increase the targeted product selectivity, reduce the undesirable thermal degradation, and facilitate product separation. Sharpless et al.[43] reported accelerated reaction rates of hydrophobic organic compounds in water and argued that the biphasic boundary between water and hydrophobic oil can also play a role. Conversely, Grunwaldt and coworkers[44-45] have investigated how various polar and non-polar solvents influence the HDO of guaiacol over Pt based catalysts and reported a higher HDO ability in presence of non-polar solvents.

To address this lack of fundamental understanding of solvent effects, we report herein an investigation of solvent influence on the reaction mechanism and possible activity descriptors for the HDO of guaiacol over a Ru(0001) model surface. Several studies conducted at relatively mild reaction conditions have reported the presence of aromatic ring saturated products[36,46] which was not considered in our previous study. Therefore, in this study, we have extended our calculations to investigate the formation of phenyl ring saturated products in vapor and condensed phases. While electrostatic interactions and hydrogen bonding contributions are instrumental for the interaction between a polar adsorbate and a polar solvent, London dispersion forces play a crucial part for non-polar adsorbate-solvent systems. To consider both of these effects, four different solvents of varying degree of polarity (dependent on Kamlet and Taft's solvatochromic parameters) have been employed for this study.[47] Specifically, we focused on the effects of liquid water which is a polar, protic solvent, 1-butanol, a polar aprotic solvent, diethyl ether, a 'borderline' polar aprotic solvent, and a non-polar solvent, n-hexane. Using first principles calculations and a novel implicit solvation scheme for solid surfaces (iSMS),[48] we characterized the solvent effects on the thermodynamics and kinetics of elementary reactions. It should be noted here that hydrogen bonding contributions are implicitly parameterized in the Conductor like Screening Model (COSMO)[73,74] and that iSMS has been shown to perform reasonably well for neutral species[100] and for reactions when hydrogen bonding contributions do not change significantly along the reaction coordinate.[50,101] A mean field microkinetic reactor model was then developed to reexamine the most abundant surface intermediates, dominant reaction pathways, and general kinetic trends in the condensed phases. We conclude our findings with a deliberation of our hypotheses and suggest further research. To the best of our knowledge, no theoretical report on solvent effects on the catalytic hydrodeoxygenation of guaiacol over transition metals catalysts has yet been published.

2. Computational Approach

2.1 Solvation Model

Solvent molecules can affect activity and selectivity of a heterogeneously catalyzed reaction in a number of ways, it can 1) compete with the adsorbed moieties for the active catalyst sites, 2) directly involve itself in the reaction coordinate, thereby providing lower energy pathways, for example, Grotthuss mechanism,[49] and 3) affect the stability of the charged intermediates or transition states. While computational investigations of chemical reactions occurring at solid-liquid interfaces can be very challenging,[50] in this study, the liquid phase effect has been approximated by employing the iSMS method.[48] A detailed discussion about the iSMS methodology and validation can be found elsewhere.[48,50-54]

The fundamental idea behind the iSMS methodology is to include long-range metallic interactions through periodic-slab models in the absence of solvent molecules and to represent the liquid phase effect as a perturbation on the (free) energy differences which is described by (sufficiently large) cluster models embedded in an isotropic continuum of constant dielectric. Consequently, the free energy function of a moiety adsorbed on a periodic metal slab submerged in liquid can be illustrated using the following subtraction scheme,

$$G^{liquid}_{surface\,+\,intermediate} = G^{vacuum}_{surface\,+\,intermediate} + (G^{liquid}_{cluster\,+\,intermediate} - E^{vacuum}_{cluster\,+\,intermediate}) \quad (1)$$

where $G^{vacuum}_{surface\,+\,intermediate}$ is the free energy of the adsorbed moieties in vapor phase, $G^{liquid}_{cluster\,+\,intermediate}$ is the free energy of the surface cluster model immersed in an implicit solvent which is fashioned by extracting selected metal atoms and removing the periodic boundary conditions, and $E^{vacuum}_{cluster+intermediate}$ is the DFT energy of the same cluster in absence of any fluid phase environment, i.e., solvation effects are captured by the term in the bracket of Eq. 1. The Conductor-like Screening Model for Real Solvents (COSMO-RS)[55] approach using the COSMOtherm program package[56] has been employed to compute $G^{liquid}_{surface+intermediate}$. Solvent thermodynamic properties are readily available in the COSMOtherm database,[56] which are based on the quantum chemical COSMO calculations at the BP-TZVP level of theory. For any other adsorbed moiety, the COSMO-RS input file was generated with the help of COSMO calculations at the same level of theory. We note that COSMO-RS is specifically parameterized for the BP-TZVP level of theory.

2.2 Periodic and Non-periodic DFT Calculations

The catalyst model investigated in this study has been explored earlier for the vapor phase hydrodeoxygenation of guaiacol over a Ru(0001) model surface,[42] and we encourage the interested readers to review the methods section of that article for a comprehensive summary of the computational details employed to perform the periodic plane-wave DFT calculations. However, it has been demonstrated recently that the Bayesian error estimation functional with van der Waals correction (BEEF-vdW)[57] performs significantly better for calculating the adsorption energies of larger adsorbates[58-59] as well as simple adsorbates such as CO[60-61] in comparison to the PBE functional[62] with dispersion corrections that we used previously.[63] Hence, the energetics of the adsorption-desorption processes as well as the all the elementary steps of the phenol hydrogenation network investigated in this study have been computed utilizing the BEEF-vdW functional. All periodic DFT calculations have been performed using the VASP[99] program package and non-periodic cluster model DFT calculations have been performed using the TURBOMOLE 6.5[64-65] program package. The cluster surfaces have been constructed by removing the periodicity of the geometries obtained from plane-wave DFT calculations and modeled as a 5×5 surface with 2 layers of metal atoms which we found to lead to converged solvation effect data with regards to cluster depth and size. Atoms that comprise the adsorbate molecules have been described by employing all electron basis sets of triple-ζ quality,[66] while a relativistic effective small core potential (ECP) combined with a basis set of the same quality as the adsorbate atoms have been employed for the valence electrons of the metal (Ru) atoms.[67] Electron exchange and correlation terms of DFT have been described by utilizing the BP86 functional[68-69] and coulomb potentials were approximated in conjunction with the RI-J approximation using auxiliary basis sets.[70-71] Single point energy calculations have been performed for the cluster models using a self-consistent field energy convergence criterion of 1.0×10^{-7} Ha with an m4 spherical grid.[72] Multiple spin states were investigated for each cluster model to identify the lowest energy spin state. For the lowest energy spin state, Conductor like screening model calculations (COSMO)[73-74] were performed where the solute molecule is embedded in a molecule shaped cavity surrounded by a dielectric medium of infinite dielectric constant (hence Conductor). Finally, the dielectric constant was scaled down to the respective dielectric constant of the solvents by utilizing the COSMO-RS[56] program package to obtain the solvation energy. Considering the ambiguity associated with the interpretation of the cavity radius of transition metal atoms in implicit solvation models (due to a lack of available experimental data),[50,75] all calculations have been repeated with a 10% incremental change on the default cavity radius of the Ru atoms.

2.3 Solvents Investigated

The HDO of guaiacol has previously been studied experimentally for the pure reactant diluted in water, diethylether, decane, octanol, hexadecane, and tetrahydrofuran.[44,76-78] In organic chemistry, it is often attempted to understand solvent effects by the *polarity* of the solvent, which can be very challenging to convey quantitatively. Empirical estimation of solvent polarity has been calculated based on linear free energy relationships of substituent solvent parameters and equilibrium, kinetic, and spectroscopic measurements.[47] By employing a solvatochromic comparison method in linear solvation energy relationship (LSER) theory, Kamlet and Taft presented a set of solvent parameters to establish a solvent polarity scale, namely, π^*, α, and β, which are related to distinct configurational properties in solution, e.g., solubilities, partition coefficients, thermodynamic and kinetic properties of chemical reactions, etc.[79-81] They correlated solvent dependent physicochemical properties of a given solvent and a reference solvent by introducing some solvent independent coefficients (s, a, b) which specify the susceptibility of the corresponding parameters, dipolarity/polarizability (π^*), hydrogen-bond donor acidities (α), and hydrogen-bond acceptor basicities (β), respectively. Table-S1 in the supporting information includes the Kamlet-Taft solvent parameters as well as the normalized solvent polarity parameter (E_T^N) for the four different solvents explored in this study, i.e., water, 1-butanol, diethylether, and n-hexane. The recorded values clearly indicate that water is the most polar protic solvent with high polarizability and hydrogen bond donating ability while n-hexane lies at the other end of the spectrum with no hydrogen bond accepting/donating capability. 1-butanol and diethylether lie in between the above mentioned two as evidenced from their normalized polarity values.

3. Model Development

3.1 Microkinetic Modeling

To analyze the implication of reaction energies and the reaction pathways under realistic processing conditions, a mean-field microkinetic model was formulated. The formulation of the partition function in the liquid phase environment is complex and dynamic contributions to the free energy of the solute are in general insensitive to whether the solute vibrational frequencies are computed in the gas phase or in the solution. Thus, in the parameterization of implicit solvation models, the vibrational partition function is often computed for the gas phase species. Hence, the zero-point corrections to the 0 K energies and vibrational partition functions under the harmonic approximation were calculated using the vibrational frequencies (ν_i) obtained from vapor phase periodic plane-wave DFT calculations.

$$E_{ZPE} = \frac{1}{2}\sum_{i} h\nu_i \tag{2}$$

$$q_{vib} = \prod_{i} \frac{1}{1 - \exp\left(\frac{h\nu_i}{k_B T}\right)} \tag{3}$$

It should be noted here that the frequency calculations include relaxations of only adsorbed moieties which result in a reduction of the accuracy of low-lying frequencies that are coupled with surface metal atoms. Considering the accuracy of DFT (or lack thereof) and the inadequacy of the harmonic approximation to describe low-lying frequencies, we established a 100 cm^{-1} cutoff value for frequencies (real) that lie below the aforementioned value. This accommodation was not required for the gas phase molecules since the rotational and the vibrational partition functions were rigorously calculated using statistical mechanics.[82]

To account for the liquid phase environment, the solvation free energy obtained from COSMO-RS calculations were utilized to reparametrize the microkinetic model. For the adsorption/desorption processes,

$$\Delta G_{solvent} = \Delta G_{gas} + G_{ads}(solv) - G_{Ru}(solv) \tag{4}$$

where $G_{ads}(solv)$ and $G_{Ru}(solv)$ are the free energies of solvation of a Ru cluster with and without an adsorbate, respectively. It is worth mentioning here that the chemical potential of all the gas phase species in a particular solvent is given by the partial pressure (fugacity) of that species in the vapor phase which is in equilibrium with the solvent phase, i.e., we assumed gas-liquid equilibrium in the absence of any mass transfer limitations. The free energy of reaction ($\Delta G_{solvent}^{rxn}$) and free energy of activation ($\Delta G_{solvent}^{\ddagger}$) of the elementary surface reactions were calculated as,

$$\Delta G_{solvent}^{rxn} = \Delta G_{gas}^{rxn} + G_{FS}(solv) - G_{IS}(solv) \tag{5}$$

$$\Delta G_{solvent}^{\ddagger} = \Delta G_{gas}^{\ddagger} + G_{TS}(solv) - G_{IS}(solv) \tag{6}$$

where the subscripts IS, TS, and FS denote the initial, transition, and final state, respectively. All reactions were presumed to be reversible reactions. Forward rate constants were calculated using harmonic transition state theory (hTST)[83] for all surface mediated elementary processes.

$$k_{forward} = \frac{\gamma k_B T}{h} \exp\left(\frac{-\Delta G^{\ddagger}}{k_B T}\right) \tag{7}$$

Here, $\Delta G^{\ddagger}$ is the free energy of activation, T is the absolute temperature, γ is the transmission coefficient, which was assumed to be 1.0 for all cases, and k_B and h are the Boltzmann and Planck constants, respectively. Collision theory was employed for calculating the forward rate constants of non-activated adsorption processes.

$$k_{forward} = \frac{\sigma}{N_o \sqrt{2\pi m k_B T}} \tag{8}$$

Here, σ stands for the sticking probability (assumed to be 1.0 for all cases), N_o is the number of catalytic sites per unit surface area, and m is the molecular weight of the adsorbate. Thermodynamic consistency was ensured by calculating the reverse rate constants from thermodynamic equilibrium constants.

$$K_{eq} = \exp\left(\frac{-\Delta G^{rxn}}{k_B T}\right) \tag{9}$$

$$k_{reverse} = \frac{k_{forward}}{K_{eq}} \tag{10}$$

Finally, with all the rate parameters known, a microkinetic reactor model was developed as a system of differential algebraic equations (DAEs). The fractional coverage of a surface intermediate at steady state is given by,

$$\frac{d\theta_i}{dt} = \sum_j \nu_{i,j} r_j = 0 \tag{11}$$

where index i refers to the ith adsorbed species and index j loops over all the elementary reactions. Furthermore, the total number of catalytic sites were conserved, and the overall site balance equation was employed to calculate the fractional coverage of empty sites.

$$\sum_i n_i \theta_i = 1 \tag{12}$$

A complete list of the number of sites assigned to each species (n_i) can be found in our vapor phase study.[42] All microkinetic models were initialized with a clean Ru surface and solved as a system of DAEs to achieve fractional surface coverages and turnover frequencies (TOFs) at steady state under realistic processing conditions.

3.2 Adsorbate-adsorbate Interactions

Adsorbate-adsorbate interactions can play a significant role for the adsorption strength as well as the stability of the adsorbed moieties which in turn can affect catalytic activity of transition metal catalysts.[54,75,84-85] Getman et al.[86-87] demonstrated a remarkable change in NO_2 dissociation capability of Pt(111) when the O coverage is typical for NO oxidation catalysts. As reported in our vapor phase study,[42] without considering any adsorbate-adsorbate interactions, H, CO, and phenoxy (C_6H_5O) become the most abundant surface intermediates when solving the microkinetic modeling equations. Hence, to mimic the local chemical environment dependence of adsorption energy in a realistic reaction environment, lateral interaction functional forms have been included in our microkinetic model. While the true description of adsorbate-adsorbate interactions can be very complicated and computationally demanding to realize, we employed the two-parameter lateral interaction model proposed by Grabow et al.[88] considering its simplicity. Table S2 of the supporting information includes the functional forms of the lateral interactions introduced in our microkinetic models. A detailed description of the calculation procedure to obtain these functional forms have been discussed in our vapor phase investigation.[42]

4. Results and Discussion

Experimental studies have reported a range of alicyclic and aromatic products for the HDO of guaiacol such as 2-methoxy-cyclohexanol, cyclohexanol, cyclohexanone, cyclohexane, benzene, catechol etc. with phenol being a major intermediate detected at short reaction times.[28,30,33,36,46] Therefore, in this study, we aim to describe the HDO of guaiacol over Ru(0001) catalysts in two steps. At first, we carried out our study in condensed phase to verify the formation of phenol from the hydrodeoxygenation of guaiacol. Next, we examine the possibility of phenyl ring saturation in vapor and condensed phases to produce two major products observed in experimental studies, cyclohexanol and cyclohexanone from phenol.[78,89-92]

4.1 HDO of Guaiacol to Unsaturated Aromatics

4.1.1 Solvent Effects on the Adsorption Strength of Reaction Intermediates

The introduction of a solvent using a continuum solvation model can alter the adsorption strength of reaction intermediates in two different ways, i) incorporating an implicit solvent introduces the previously unaccounted for adsorbate-solvent interaction, and ii) it modifies the metal-adsorbate interaction by changing the electronic structure of the metal due to indirect solvent-metal interactions. Solvent induced changes in the adsorption strength of a reaction intermediate can significantly affect the overall activity of a catalyst site by modifying the activation and reaction free energies. To investigate the effects of solvent on the adsorption strength of the intermediates involved in the HDO of guaiacol, we computed the difference in adsorption free energy in the absence and presence of a solvent,

$$A(g) + *(g) \leftrightarrow A*(g) \tag{13}$$

$$A(g) + *(l) \leftrightarrow A*(l) \tag{14}$$

$$\begin{aligned} \Delta(G_{ads,A}) &= G_{ads,A}(l) - G_{ads,A}(g) \\ &= \left[G^{A*}(l) - G^{A*}(g)\right] - \left[G^{*}(l) - G^{*}(g)\right] = \Delta(\Delta G) \end{aligned} \tag{15}$$

where, $G_{ads,A}(l)$ and $G_{ads,A}(g)$ are the free energies of adsorption of a gas molecule of intermediate A in the presence and absence of the solvent, $G^{A*}(l)$ and $G^{A*}(g)$ are the free energies of the adsorbed moiety A in the presence and absence of solvent, and $G^{*}(l)$ and $G^{*}(g)$ are free energies of the clean surface model in the presence and absence of solvent, respectively. It should be noted here that while many adsorbed moieties can be unstable when separated from their adsorption site; nonetheless, this scheme permits us to compare the relative adsorption strength in a liquid phase environment with respect to the gas phase adsorption strength. Using this procedure, we essentially use an ideal gas phase as reference state for all species and assume equilibrium between the molecules in the liquid phase and a hypothetical gas phase, i.e., we are assuming fast mass transfer. The activity coefficient/fugacity of the molecules in the liquid phase at a given concentration in the various solvents is computed using COSMOtherm.

The investigated surface moieties in the reaction network of the HDO of guaiacol and the calculated change in their adsorption strength in various reaction environments are listed in Table 1. In total, we investigated 39 surface intermediates in our reaction network that includes guaiacol, phenol, catechol, and their derivatives. Snapshots of all adsorbed geometries can be found in our previous vapor phase study.[42] For the convenience of comparison of the solvent effect on the adsorption strength of the surface intermediates, we classified the intermediates into four different classes of structurally similar species where all the species belonging to a class display similar trends in solvent effects across all four solvents studied in this paper.

Class I: Guaiacol and Its Derivatives

Presence of a liquid-phase environment significantly stabilizes the adsorption of guaiacol on Ru(0001) sites ($\Delta(\Delta G^{water}) = -0.22\ eV$,$\Delta(\Delta G^{1-butanol}) = -0.47\ eV$, $\Delta(\Delta G^{diethylether}) = -0.43\ eV$, $\Delta(\Delta G^{n-hexane}) = -0.33\ eV$). Solvents employed in this study can be arranged in the order of their effect on the adsorption strength of guaiacol and its dehydrogenated and partially hydrogenated derivatives as 1-Butanol > Diethyl ether > n-Hexane > Water. This phenomenon can be attributed to the fact that guaiacol has a large non-polar aromatic ring with a polar hydroxyl group and slightly polar methoxy group. The presence of a polar solvent (Water) ensures favorable solute-solvent interaction, i.e., formation of hydrogen bonds, thereby increasing the adsorption strength of guaiacol and its derivatives. Reducing the polarity of the solvent (1-Butanol, Diethyl ether) enhances the stabilization of the adsorption strength of these species because of the additional favorable interaction between non-polar fragments of the solute and solvent due to increased London forces while retaining some of the favorable interaction between polar fragments of the solute and solvent. For non-polar aprotic solvents such as n-hexane, the stabilization of the adsorption strength only comes from the favorable solute-solvent interaction due to London dispersion forces, which reduces the solvent effect on the adsorption strength of guaiacol and its derivatives compared to that of 1-butanol and diethyl ether. Partially hydrogenated ($C_6H_4H_{\alpha/\beta}(OH)(OC_xH_y)$), x=[0,1], y=[0,3]) and dehydrogenated ($C_6H_4(O_vH_w)(O_xC_yH_z)$), v=[0,1], w=[0,1], x=[0,1], y=[0,1], z=[0,3]) species of guaiacol all maintain the same order of the solvent effect on the adsorption strength. For example, the 2-methoxy-phenyl ($C_6H_4(OCH_3)$) intermediate can be produced by $C_{aryl(\alpha)}$-OH bond scission of guaiacol. Due to the loss of a polar hydroxyl group, the solvent stabilization of the adsorption strength in water gets reduced ($\Delta(\Delta G^{water}) = -0.07\ eV$) compared to that of guaiacol, while the increasingly non-polar solvents such as 1-butanol, diethyl ether and n-hexane retain most of the solvent stabilization ($\Delta(\Delta G^{1-butanol}) = -0.35\ eV, \Delta(\Delta G^{diethylether}) = -0.33\ eV, \Delta(\Delta G^{n-hexane}) = -0.24\ eV$) that is due to dispersion forces between non-polar fragments of the solute and solvent.

Class II: Phenol, Anisole, Catechol, Benzene and Their Derivatives

Phenol, due to the presence of a strongly polar hydroxyl group, displays a significant solvent stabilization in aqueous phase ($\Delta(\Delta G^{water}) = -0.20\ eV$), and the presence of a non-polar aromatic ring ensures an increase in adsorption strength for other solvents with various degree of polarity ($\Delta(\Delta G^{1-butanol}) = -0.38\ eV, \Delta(\Delta G^{diethylether}) = -0.35\ eV, \Delta(\Delta G^{n-hexane}) = -0.26\ eV$). On the other end of the spectrum, benzene, being non-polar, shows a small solvent stabilization in its adsorption strength in the aqueous phase (($\Delta(\Delta G^{water}) = -0.10\ eV$). However, benzene shows a sizable solvent stabilization in adsorption strength in the other solvents due to favorable solute-solvent London dispersion interaction ($\Delta(\Delta G^{1-butanol}) = -0.26\ eV, \Delta(\Delta G^{diethylether}) = -0.24\ eV, \Delta(\Delta G^{n-hexane}) = -0.17\ eV$). Overall, phenol ($C_6H_5OH$), anisole ($C_6H_5OCH_3$), catechol ($C_6H_4(OH)_2$), benzene ($C_6H_6$), and their dehydrogenated surface intermediates follow the same order of solvent stabilization as mentioned before for guaiacol species.

Class III: Methane and Its Derivatives

Methane and its dehydrogenated derivatives such as methyl (CH_3), methylene (CH_2), and methylidyne (CH) display a marginally weaker adsorption strength in the aqueous phase due to their non-polar nature. For example, the adsorption strength of methane in liquid water decreased by 0.04 eV. We also find that the adsorption strength of methane and its derivatives is hardly affected by the presence of other solvents such as 1-butanol, diethyl ether, and n-hexane.

Class IV: Methanol and Its Derivatives

Presence of liquid water weakens the adsorption strength of strongly polar methanol and its dehydrogenated species methoxy (CH_3O) ($\Delta\left(\Delta G_{methanol}^{water}\right) = 0.12\ eV, \Delta\left(\Delta G_{methoxy}^{water}\right) = 0.09\ eV$). This inverse solvent effect on a polar species can be rationalized by observing their binding modes and their strongly polar nature. Both methanol and methoxy species binds to the Ru(0001) surface through the O atom, a hydrogen bond donor. Due to their polar nature, these species have a favorable solute-solvent interaction in polar solvents (through hydrogen bonding) which in turn weakens solute-surface interaction, thereby reducing the adsorption strength when following bond order conservation principles. As we decrease the polarity of the solvents, the adsorption strength gets stabilized. For less polar dehydrogenated species such as formaldehyde (CH_2O) and formyl (CHO), the presence of a liquid phase environment hardly affects the adsorption strength.

4.1.2 Solvent Effects on Elementary Processes

Figure 1 illustrates a schematic of the investigated elementary reactions involved in the HDO of guaiacol over a Ru(0001) model surface. Energetics of all adsorption/desorption reactions are reported in Table 2 using BEEF-vdW functional in different reaction environments at 473 K. Free energies of reaction and free energies of activation of all elementary surface processes in different reaction environments are listed in Table 3 for a reaction temperature of 473 K.

In the following, we discuss the solvent effects on the free energy of reaction and free energy of activation of various elementary processes involved in the HDO of guaiacol. For the convenience of comparison, the reaction pathways have been labeled from 2 to 8 according to the first reaction step labeled in Figure 1, adsorption of guaiacol being the first reaction step. Pathways

2 and 3 start with selective hydrogenation of $C_{aryl(\beta)}$ and $C_{aryl(\alpha)}$ of guaiacol, respectively. Direct removal of a hydroxyl group, methoxy group, and a methyl group from guaiacol have been considered in pathways 4, 5, and 7, respectively. Pathways 6 and 8 considers the dehydrogenation of guaiacol through C-H bond scission of the methoxy group and O-H bond scission of the hydroxyl group, respectively.

I: Selective hydrogenation of the phenyl ring

Selective hydrogenation of the phenyl ring of guaiacol to form $C_6H_4H_\beta(OH)(OCH_3)$ (step 2) and $C_6H_4H_\alpha(OH)(OCH_3)$ (step 3) are both endergonic steps in the vapor phase ($\Delta G_{rxn} = 0.40\ eV$ and $\Delta G_{rxn} = 0.51\ eV$, respectively) and kinetically demanding with a free energy of activation of 1.10 eV and 1.14 eV, respectively, which makes pathways 2 and 3 unfavorable. Liquid solvents employed in this study (water, 1-butanol, diethyl ether, and n-hexane) have an unfavorable effect on the free energies of $C_{aryl(\beta)}$-H hydrogenation, making it more endergonic (free energy of reaction ranging from 0.41 eV to 0.49 eV) and making it kinetically more demanding. Liquid water does not have any effect on the free energy of reaction of $C_{aryl(\alpha)}$-H hydrogenation, with a minimal increase in the free energy of activation ($\Delta(\Delta G^\ddagger)$=0.04eV). Employing other solvents such as 1-butanol, diethyl ether, or n-hexane have a minimal exergonic effect on the free energy of reaction with a slight increase in the free energy of activation ($\Delta(\Delta G^\ddagger_{1-butanol}) = 0.06$eV, $\Delta(\Delta G^\ddagger_{diethyl\ ether}) = 0.06$eV, $\Delta(\Delta G^\ddagger_{n-hexane}) = 0.07$eV).

Similar to the vapor phase, further dehydrogenation of the methoxy group (step 9) remains challenging compared to the methoxy group removal (step 10) of $C_6H_4H_\beta(OH)(OCH_3)$ in all solvents studied. Liquid water increases the free energy of activation of the subsequent methylene group removal (step 23) process by 0.16 eV while it remains largely unaffected in all other solvent media. The energetics of the hydrogenation of the resulting $C_6H_4H_\beta(OH)(O)$ species to produce

$C_6H_5(OH)_2$ (step 36) also show only a minimal perturbation from the vapor phase for different solvent media. The final step to produce phenol involves dehydroxylation of the phenyl ring (step 41) and employing increasingly non-polar solvents makes this step more facile by 0.11-0.15 eV.

Less protic solvent media such as 1-butanol, diethyl ether, and n-hexane have an endergonic effect on the free energy of activation for the dehydroxylation of the $C_{aryl(\alpha)}$ hydrogenated species of guaiacol (step 11) to produce anisole while the energetics remain unchanged in water compared to that of vapor phase. Different reaction media also exert a limited effect on the kinetics of the subsequent dehydrogenations of anisole (step 24 and step 37). Overall, the energetics of pathways 2 and 3 suggest that HDO of guaiacol does not proceed through selective hydrogenation of the phenyl ring, similar to the vapor phase, which agrees with experimental observations.[28]

II: Direct removal of functional groups

Pathways 4, 5, and 7 consider direct removal of -OH, -OCH_3, and -CH_3 functional groups, which were found to be kinetically difficult in the vapor phase and which remain difficult in liquid phase environments. A liquid phase environment exerts an endergonic effect on the thermodynamics of the removal of the hydroxyl species from guaiacol to produce 2-methoxy phenyl species ($C_6H_4OCH_3$) (step 4). While the presence of an aqueous phase increases the free energy of activation by 0.07 eV, other solvent media hardly affect the kinetics of the reaction. Subsequent hydrogenation to anisole, however, gets more exergonic in the liquid phase environment with water contributing the most $\Delta(\Delta G_{rxn}) = -0.22\ eV$) while the kinetics also become slightly facilitated.

In the methoxy group removal pathway (pathway 5), the removal of the -OCH_3 species (step 5) becomes kinetically more unfavorable in water ($\Delta(\Delta G^{\dagger})$=0.07eV) while other solvents have a minimal effect. Subsequent hydrogenation of the 2-hydroxy phenyl species (C_6H_4OH) to produce phenol (step 13) becomes thermodynamically more favorable in the liquid phase environment compared to that of the vapor phase.

The seventh pathway consists of removal of a methyl group from guaiacol to produce a hydrogen catecholate species ($C_6H_4(OH)(O)$) (step 7) which is highly exergonic in the vapor phase ($\Delta G_{rxn} = -1.35\ eV$). Introduction of a liquid phase environment has an endergonic effect on the thermodynamics of the reaction while the kinetics remains mostly unchanged. The hydrogen catecholate can be hydrogenated to catechol (step 18) which remains largely unchanged in liquid water, while less protic solvents have a favorable effect on both the thermodynamics and the kinetics of this elementary process. Catechol can be either dehydroxylated to a 2-hydroxy phenyl species (C_6H_4OH) (step 27) or hydrogenated to produce a $C_6H_5(OH)_2$ species (step 28) which are both kinetically very demanding. Presence of a liquid phase environment does not affect the kinetics of these processes while having minimal effect on the thermodynamics.

In summary, a liquid phase environment does not help these kinetically demanding processes of direct functional group removal to make them more facile.

III: Dehydrogenation of methoxy and hydroxyl groups

In pathways 6 and 8, we discuss the initial dehydrogenation of the -OCH_3 and -OH groups of guaiacol. The removal of a hydrogen from the methoxy group of guaiacol to produce the 2-methylene-oxy-phenol intermediate ($C_6H_4(OH)(OCH_2)$) (step 6) is both thermodynamically and kinetically favorable in the vapor phase ($\Delta G_{rxn} = -0.36\ eV, \Delta G^{\ddagger} = 0.50\ eV$). Introduction of an aqueous phase has an endergonic effect on the free energy of reaction ($\Delta(\Delta G_{rxn}) = 0.09\ eV$) with negligible impact on the free energy of activation ($\Delta(\Delta G^{\ddagger}) = 0.02\ eV$). All the other less protic solvents (1-butanol, diethyl ether, and n-hexane) have a less endergonic effect on the thermodynamics of the reaction compared to water ($\Delta(\Delta G_{rxn}) = 0.04\ eV$) with the kinetics remaining unperturbed. 2-methylene-oxy-phenol species can go through -OCH_2 removal (step 14), dehydrogenation at the hydroxyl group (step 15), dehydrogenation of the methylene group (step 16), and removal of -CH_2 (step 17). The most facile path in the vapor phase is dehydrogenation of the methylene group (step 16) ($\Delta G_{rxn} = -0.53\ eV, \Delta G^{\ddagger} = 0.02\ eV$), which remains unchanged in the liquid phase environment. However, while the liquid phase environment does not affect the free energy of reaction of this elementary step, the free energy of activation is perturbed differently for polar and non-polar solvents. The reaction becomes barrierless in an aqueous phase while for other solvents, the free energy of activation increases by 0.10 eV compared to that of the vapor phase. The product of step 16, 2-methylidyne-oxy-phenol ($C_6H_4(OH)(OCH)$) can then either undergo methyne (-CH) removal to produce a once hydrogenated catecholate intermediate ($C_6H_4(OH)O$) (step 26) or formyl (-OCH) removal to produce a 2-hydroxy-phenyl species (C_6H_4OH) (step 25). Step 26 is much more facile compared to step 25 in the vapor phase which remains consistent in the presence of a liquid phase environment. However, while liquid water makes the process more exergonic by 0.09 eV, other less protic solvents makes it more endergonic by 0.17 eV compared to that of the vapor phase. Elementary processes involving the $C_6H_4(OH)O$ species have already been discussed in the previous section and consequently will not be discussed further.

Finally, the pathway eight, which involves dehydrogenation of the hydroxyl group of guaiacol to produce a guaiacolate intermediate($C_6H_4(O)(OCH_3)$) (step 8) is the most facile reaction pathway in the vapor phase ($\Delta G_{rxn} = -0.77\ eV, \Delta G^{\ddagger} = 0.29\ eV$). In the liquid phase, all solvents pose an endergonic effect on the free energy of reaction of this elementary process by ~0.10 eV. The free energy of activation remains unaltered in less protic solvents while liquid water shows an endergonic effect ($\Delta(\Delta G^{\ddagger}) = 0.08\ eV$) making this step competitive with the dehydrogenation of the methoxy group of guaiacol (step 6). Next, the methoxy group is dehydrogenated (step 22) which is more facile ($\Delta G_{rxn} = -0.32\ eV, \Delta G^{\ddagger} = 0.53\ eV$) compared to the alternative step which involves complete removal of the methoxy group (step 21) ($\Delta G_{rxn} = 0.21\ eV, \Delta G^{\ddagger} = 1.08\ eV$) in the vapor phase. Liquid water further facilitates the kinetics of the methoxy group dehydrogenation step (step 22) ($\Delta(\Delta G^{\ddagger}) = -0.06\ eV$). The product of step 22, 2-methylene-oxy-phenolate ($C_6H_4(O)(OCH_2)$) then undergoes a barrierless dehydrogenation reaction (step 33) across all reaction environments to produce a 2-methylidyne-oxy-phenolate ($C_6H_4(O)(OCH)$) species where the thermodynamics of the process becomes slightly exergonic (by ~0.05 eV) when using less protic solvents compared to that of the vapor phase. In the vapor phase, two kinetically competing reactions develop at this point, methylidyne (-CH) removal (step 34) and hydrogen removal (step 35) from the $C_6H_4(O)(OCH)$ intermediate. In the liquid phase environment, the reactions become even more competitive, i.e., the difference between the free energy of activation of these two elementary processes in 1-butanol solvent is only 0.07 eV. The product of step 34, a catecholate species ($C_6H_4O_2$) then undergoes hydrogenation (step 42) which connects the eighth pathway with the sixth at this point. The product of the other elementary step (step 35), 2-carbide-oxy-phenolate ($C_6H_4(O)(OC)$), then goes through decarbonylation (step 43) to produce a 2-oxyphenyl (C_6H_4O) intermediate. While the kinetics of this reaction mostly remains unperturbed due to the presence of a liquid phase, the free energy of reaction becomes more endergonic ($\Delta(\Delta G_{rxn}) = 0.21\ eV$) in liquid water while other less protic solvents makes this process more exergonic ($\Delta(\Delta G_{rxn}) = -0.08\ eV$). Lastly, the C_6H_4O species gets hydrogenated to phenol (C_6H_5OH) (step 30) and an aqueous phase environment facilitates this process both thermodynamically ($\Delta(\Delta G_{rxn}) = -0.12\ eV$) and kinetically ($\Delta(\Delta G^{\ddagger}) = -0.09\ eV$).

Based on the thermodynamics and kinetics of the elementary processes, we can presume that the dominant reaction pathway of the vapor phase (pathway 8) remains dominant in all condensed phase reaction media. However, any computational catalysis study based on only free energies remains inadequate for not considering the realistic reaction conditions and not predicting the experimental observables to which it can be compared directly. Therefore, in the following sections, we investigate the effect of solvents on the turn-over frequency (TOF) and the coverage of the most abundant surface intermediates through mean-field microkinetic modeling.

4.1.3 Mean-field Microkinetic Modeling

In our previous study, we investigated the vapor phase kinetics of the HDO of guaiacol over a Ru(0001) surface[42] where we found that at low hydrogen partial pressure and moderate reaction temperature (573K), kinetically the most favorable pathway proceeds through dehydrogenation of the hydroxyl group of guaiacol (pathway 8) and the major reaction product was phenol with catechol as the most relevant side product. In this study, we extend our microkinetic model to account for the effect of solvation by including the change in free energy of reaction and free energy of activation due to the presence of a condensed phase. We utilized the experimental reaction conditions of 0.50 g of guaiacol in 10 g of solvent under relatively mild reaction conditions (473 K) and 15 bar partial pressure of H_2, similar to the reaction conditions of Tomishige et al.[36,46] To find the corresponding fugacity/partial pressure of guaiacol, we utilized the modified Raoult's law,

$$f_{gua}^{v} = P_{gua} = x_{gua}\gamma_{gua}P_{gua}^{sat} \qquad (16)$$

Thermodynamic data such as activity coefficient, saturation pressure of guaiacol, and fugacity of pure solvent have been calculated using the COSMOtherm program package.[73-74] We calculated the guaiacol fugacity to be 0.94 bar, 0.03 bar, 0.02 bar, and 0.05 bar in liquid water, 1-butanol, diethyl ether, and n-hexane, respectively at 473 K and assuming 1% conversion, the phenol partial pressure was set accordingly. For vapor phase simulations, we used a guaiacol chemical potential/fugacity corresponding to the one in liquid water. Using low conversion conditions to other reaction products such as catechol, anisole, and benzene, their partial pressures were set at 10^{-6} bar. We chose a slightly higher partial pressure of CO (10^{-4} bar) to observe the poisoning effect of CO on the reaction mechanism, similar to our prior research.[42] For all simulations, we employed the same coverage dependent adsorption energies as reported in our previous contribution[42] for the three most abundant surface intermediates of the vapor phase, H, CO, and phenoxy (C_6H_5O). A summary of our calculated TOFs at four different reaction temperatures and at various reaction environments are presented in Table 4.

I. Liquid Water Effects

In the presence of an aqueous phase at 473 K (i.e., at a corresponding equilibrium water partial pressure of 15.536 bar), we observe that the surface is predominantly covered with CH, CO, H, and phenoxy (C_6H_5O) species (Table 5). The computed overall TOF decreases by a factor of 2.9 going from the vapor phase ($TOF_{overall\text{-}vapor} = 1.95 \times 10^{-4}$ s^{-1}) to an aqueous phase ($TOF_{overall\text{-}water} = 6.70 \times 10^{-5}$ s^{-1}). The calculated TOFs along the dominant reaction pathway in different reaction environments are shown in Figure 2. The major product in the aqueous phase is predicted to be phenol ($TOF_{phenol} = 6.66 \times 10^{-5}$ s^{-1}), similar to the vapor phase.[42] However, unlike the vapor phase where catechol was found to be the major side product, in liquid water we found benzene to be the major side product with a two order of magnitude lower production rate than that of phenol ($TOF_{benzene} = 4.02 \times 10^{-7}$ s^{-1}) which agrees qualitatively well with experimental studies.[10,46]

As we have reported previously,[50,75] a fundamental caveat of using a continuum solvation scheme to compute the solvent effects is the uncertainty associated with the cavity radius of transition metal atoms due to a lack of accurate experimental solvation data. To account for the uncertainty of Ru atoms, we performed our aqueous phase calculations at three different cavity radii of Ru atoms: the default cavity radius provided by the TURBOMOLE[64] program package (2.223 Å), a 10% increased cavity radius (2.445 Å), and a 10% decreased cavity radius (2.0007 Å). Our microkinetic model results indicated that the usage of a different cavity radius does not change the dominant reaction mechanism in an aqueous phase. However, we also observed that the overall TOF decreases by 2 orders of magnitude ($TOF_{water}^{COSMO\,-\,10}= 1.35 \times 10^{-7}$ s^{-1}) when we decrease the cavity radius of Ru atoms while with a 10% increase, TOF increases by a factor of 1.22 ($TOF_{water}^{COSMO\,+\,10}= 8.19 \times 10^{-5}$ s^{-1}).

Hellinger et al.[44] studied the solvent effect on the HDO of guaiacol over Pt/SiO_2 and Pt/H-MFI 90 catalysts at 450 K and 50 bar hydrogen partial pressure. They surmised that polar solvents lead to a lower conversion of the HDO of guaiacol due to the oxygen containing solvents being strongly adsorbed on the active sites of the catalysts leading to blockage of active sites,[93] which partially explains why our model predicted a lower activity of the Ru catalyst in an aqueous phase. Nakagawa et al.[36] investigated of HDO of guaiacol over Ru/C catalysts in aqueous phase at a relatively low temperature (433K) and 15 bar H_2 partial pressure. The major products they observed are phenyl ring saturated products such as cyclohexanol, 2-methoxycyclohexanol, and cyclohexane. Addition of MgO to the reaction media increased the yield of cyclohexanol and methanol. Using the same reaction conditions, Ishikawa et al.[46] studied the HDO of guaiacol over carbon black supported Ru-MnO_x catalyst (Ru-MnO_x/C) and found cyclohexanol and methanol to be the major product. However, in both cases they observed phenol at short reaction times and the selectivity of phenol decreased with guaiacol conversion and cyclohexanol production, which agrees with our calculations of the HDO of guaiacol at low conversion conditions.

II. Less Protic Solvent (1-Butanol, Diethyl ether, and n-Hexane) Effects

Microkinetic models for 1-butanol, diethyl ether, and n-hexane were performed under similar reaction conditions except that we employed a water partial pressure similar to our vapor phase simulations ($P_{H_2O} = 10^{-6}$ bar). Unlike for water, solvent adsorption is not considered in the microkinetic models since at the high reaction temperatures the (vapor phase) adsorption free energy of all solvent molecules is highly endergonic (at 473 K it is 0.31 eV for 1-butanol, 0.51 eV for diethyl ether, and 0.52 eV for n-hexane). As a result, the solvent surface coverage is smaller 10^{-2} % under all reaction conditions and does not affect the observed kinetics. Our simulations predict a factor two increase in catalytic activity ($TOF_{1-butanol} = 4.66 \times 10^{-4}$, $TOF_{diethyl\,ether} = 4.33 \times 10^{-4}$, $TOF_{n-hexane} = 5.17 \times 10^{-4}$) relative to the vapor phase ($TOF_{1-butanol} = 1.95 \times 10^{-4}$ s^{-1}) for less protic solvents which agrees with the observation of Hellinger et al.[44] that non-polar solvents have a positive effect on the HDO of guaiacol. Except for higher temperatures (>523 K), we found that the presence of a less protic solvent facilitates the phenol production. Chen et al.[76] reported phenol as an intermediate for HDO of guaiacol over Ru/C at 413-533 K and 4 MPa hydrogen partial pressure using ethanol as a solvent, which has a normalized polarity close to that of 1-butanol. Lu et al.[77] investigated the HDO of guaiacol over Ru/TiO_2, Ru/ZrO_2, and Ru supported on TiO_2-ZrO_2 composite oxides at 473-533K and 2 MPa hydrogen partial pressure using a non-polar solvent, n-dodecane as the reaction medium. They found 2-methoxycyclohexanol, cyclohexanol, and phenol to be the major reaction products at low reaction temperature (473K) which partially confirms our microkinetic model predictions.

4.1.4 Apparent Activation Barrier, Reaction Orders, and Sensitivity Analysis

We calculated the apparent activation barrier (E_a) and reaction orders (n_{gua}, n_{CO}, & n_{H_2}) (Table 6), and performed a sensitivity analysis in different reaction environments (Table 7). Going from the vapor to an aqueous phase, the estimated apparent activation barrier for the temperature range of 423 K-573 K increases by 0.03 eV which explains the decrease in TOF in liquid water. In less protic solvents such as 1-butanol, diethyl ether, and n-hexane, we predict very similar apparent activation energies of 1.55 eV, 1.57 eV, and 1.58 eV, respectively. The lower apparent activation energies in less protic solvents can be attributed to the slightly higher number of free sites available compared to that of liquid water (Table 5).

Next, we investigated the dependence of the overall TOF on the partial pressures of guaiacol, CO, and H_2, and the results have been summarized in Table 6. An increase in partial pressure of guaiacol increases the reaction rate across all reaction environments with the less protic solvents predicting same reaction order for guaiacol (0.12). Site blocking due to increase in CO partial pressure leads to a negative reaction order for CO in all reaction environments where the aqueous phase shows the most pronounced effect (n_{co}^{water}= -0.65). This phenomenon can be explained by the shift in equilibrium of the decarbonylation step 43 to the reactant (2-carbide-oxy-phenolate to 2-oxyphenyl) in liquid water, resulting in a 99.8% decrease in the TOF for the elementary step while increasing the CO partial pressure from 10^{-5} bar 0.10 bar. For less protic solvents, this reaction step does not become more endergonic but exergonic relative to the vapor phase (Table 3), partially explaining why CO poisoning is reduced in these solvents. We also observed an inhibiting effect of low H_2 partial pressure (0.20 – 0.40 bar) in vapor and aqueous phase environments. However, our model indicated that in other less protic solvents, even in the low temperature range, the hydrogen reaction order remains positive. This observation can be attributed to step 46, the CH species removal step from the surface. In vapor and aqueous phases, this reaction step poses a modest (~0.60 eV) activation barrier. In the low partial pressure region ($P_{H_2} = 0.20 - 0.40\ bar$), the slight increase in hydrogen partial pressure slightly increases the hydrogen coverage but fails to shift the equilibrium of the reaction, thereby reducing the number of free sites available which again leads to an inhibiting effect. Meanwhile, in other protic solvents, due to the low free energy of activation (0.18-0.35 eV), even a slight increase in hydrogen partial pressure is able to move the equilibrium to the right, resulting in an increased number of available free sites that promotes guaiacol adsorption and reaction. Further increase in partial pressure of hydrogen (0.60 - 20.0 bar) shifts the equilibrium to the right, thereby decreasing the poisoning effect of CH and promoting the reaction rate across all reaction environments.

To identify the rate controlling steps and surface intermediates, we used Campbell's degree of rate control and degree of thermodynamic rate control[94-96] analyses. Results of the sensitivity analyses are summarized in Table 7. We observed that H, CO, and CH have a poisoning effect on the catalyst due to their high surface coverage in vapor and aqueous phase processing conditions such that destabilizing their adsorption increases the overall reaction rate. In less protic reaction environments, the largest degree of rate controlling species was found to be $C_6H_4O_2$ which has a similar poisoning effect on the surface. Due to the high surface coverage of the CH species in vapor and aqueous phases, our model predicts methyl hydrogenation to methane as one of the rate controlling steps in the reaction mechanism. However, in less protic solvents, dehydroxylation of the hydrogen catecholate species ($C_6H_4(OH)O$) to 2-oxyphenyl (C_6H_4O), which serves as a precursor to phenol production, becomes the most rate controlling reaction such that lowering the activation barrier increases the overall reaction rate. Across all reaction environments, our model predicts that CH removal of 2-methyledyne-oxy-phenolate species ($C_6H_4(O)(OCH)$) to catecholate species ($C_6H_4O_2$) has an inhibiting effect while dehydrogenation to 2-carbide-oxy-phenolate intermediate ($C_6H_4(O)(OC)$) facilitates the overall TOF. Owing to a lack of an availability of free sites for catalysis, our model also predicts a moderate degree of rate control for the guaiacol adsorption process.

4.2 Hydrogenation of Phenol to Alicyclic Products

4.2.1 Reaction Network

The hydro-upgrading of phenol to cycloalkanes can occur in a number of different ways. Hydrogen addition steps can happen at the α-C (C_1 pathway), *ortho-* (C_2 pathway), *meta-* (C_3 pathway), or *para-* (C_4 pathway) positions of the phenolic ring to produce cyclohexanol and cyclohexanone (Figure 4 and Figure 5). Furthermore, phenol can undergo dehydrogenation to produce a phenoxy species and then go through hydrogenation steps to produce cyclohexanone. Cyclohexanone can then undergo C=O hydrogenation to form cyclohexanol (Keto-enol tautomerization pathway, Figure 6). The naming convention employed in the reaction network schemes is as follows: first hydrogenation of the phenyl ring at C_x position leads to the formation of HCX-1 intermediate species [X=1, 2, 3, 4], and subsequent hydrogenated moieties are denoted adding a second integer. Different structures with same number of hydrogenations of phenol are distinguished by adding a letter at the end. For example, HC1-3a (Figure 4) refers to an intermediate species in the C_1 hydrogenation pathway with three hydrogenations of the phenyl ring, the last of which occurs at the C_5 position, while HC1-3b refers to an adsorbed species of the same pathway with same number of hydrogenations, the last of which happening at C_6 position. Finally, cyclohexanol being a species hydrogenated at all six carbons of phenol is denoted as HC-6 species.

For the keto-enol tautomerization pathway (Figure 7), dehydrogenation of phenol at the hydroxyl group leads to the formation of a phenoxy species (KET-1). Subsequent hydrogenated products along the reaction network are denoted using an integer after 'KET', e.g., KET-5d refers the to a phenolate species that has been hydrogenated four times, the last of which occurs at C_6 position. KET-6 (Cyclohexanone) refers to complete hydrogenation of the phenolate species. In total, we investigated 114 elementary steps along the reaction network for phenol hydrogenation to cycloalkanes over a Ru(0001) surface. Table S3 of the supporting information summarizes the free energies of these elementary processes at three different reaction temperatures and Figure S1 and S2 displays the side and top views of the optimized intermediates and transition state structures investigated for this reaction network. In the following sections, we discuss the energetics of these elementary processes in vapor and condensed phases. Unless otherwise stated, the free energies of reaction and free energies of activation are interpreted at a reaction temperature of 473 K.

4.2.2 Energetics in Vapor Phase

In the C_1 pathway, addition of a hydrogen to phenol (step 1) leads to the formation of the HC1-1 species ($C_6H_5H_\alpha OH$) which is an endergonic process ($\Delta G_{rxn} = 0.41\ eV$) and requires overcoming a free energy of activation of 1.16 eV. Subsequent hydrogenation to HC1-2a (step 2, second hydrogenation at the *para*- position) or HC1-2b (step 3, second hydrogenation at the *ortho*-position) are both highly endergonic processes with free energies of reaction of 0.85 eV and 0.80 eV, respectively (See Table S3). In pathway C_2, hydrogenation of phenol (step 37) results in HC2-1 species ($C_6H_5H_{ortho}OH$) which is a thermodynamically and kinetically challenging process ($\Delta G_{rxn} = 0.58\ eV, \Delta G^{\ddagger} = 1.11\ eV$). HC2-1 can then undergo a second hydrogenation step to produce

HC2-2a (step 38) or HC2-2b (step 39) which are again thermodynamically demanding processes ($\Delta G_{rxn}^{38} = 0.62\ eV, \Delta G_{rxn}^{39} = 0.78\ eV$).

Hydrogenation of phenol at the *meta* position (Pathway C_3) leading to the formation of a HC3-1 species (step 52) is a kinetically difficult endergonic process ($\Delta G^{\ddagger} = 1.05\ eV$). Second hydrogenations of phenol along this reaction pathway to produce HC3-2a or HC3-2b moieties are also endergonic processes with free energies of reaction of 0.72 eV and 0.74 eV, respectively. Along the C_4 pathway, hydrogenation of phenol (step 77) produces the HC4-1 ($C_6H_5H_{para}OH$) species which is also an endergonic and kinetically challenging process ($\Delta G_{rxn} = 0.71\ eV, \Delta G^{\ddagger} = 1.15\ eV$).

Finally, in the keto-enol tautomerization pathway (Figure 7), the initial O-H scission of phenol at the hydroxyl group (step 80) was found to be a facile exergonic process ($\Delta G_{rxn} = -0.76\ eV, \Delta G^{\ddagger} = 0.31\ eV$). Therefore, it is most likely that phenol at first undergoes to dehydrogenation to form a phenolate species before further hydrogenations. Subsequent hydrogenations of the phenolate (KET-1) species to KET-2a (step 81) and KET-2b (step 102) are both thermodynamically challenging processes ($\Delta G_{rxn}^{81} = 0.99\ eV, \Delta G_{rxn}^{102} = 0.94\ eV$). Due to the enormity of the reaction network, we made use of the Evans-Polanyi principle[97] at this stage, which points to the favorability of step 102 over step 81 due to its less endergonicity. Thermodynamics of subsequent hydrogenations of the KET-2b species (step 103, 104, 105, and 106) predicts the most thermodynamically favorable pathway to be step 105 to produce the KET-3g species ($\Delta G_{rxn} = 0.27\ eV, \Delta G^{\ddagger} = 0.84\ eV$). Next, KET-3g is hydrogenated to KET-4d (step 109) which is an endergonic process with challenging kinetics ($\Delta G_{rxn} = 0.42\ eV, \Delta G^{\ddagger} = 1.06\ eV$). KET-4d intermediate, which is the same as KET-4b, is subsequently hydrogenated to KET-5c (step 92) or KET-5d (step 93), of which the former is thermodynamically more favorable ($\Delta G_{rxn}^{92} = 0.17\ eV, \Delta$

$G_{rxn}^{93} = 0.82\ eV$) with a free energy of activation of 1.07 eV. KET-5c then undergoes hydrogenation (step 96) to produce KET-6 (Cyclohexanone) with a moderately endergonic reaction free energy ($\Delta G_{rxn} = 0.32\ eV$) and a high free energy of activation ($\Delta G^{\ddagger} = 1.21\ eV$). KET-6 finally undergoes hydrogenation at the hydroxyl group to form KET-7a (step 98) and subsequently hydrogenated (step 100) to produce HC-6 (Cyclohexanol). Although kinetically very demanding, on the basis of these energetics calculations alone, the likely pathway to produce cyclohexanol from phenol proceeds through,

$$Phenol \rightarrow KET-1 \rightarrow KET-2b \rightarrow KET-3g \rightarrow KET-4b \rightarrow KET-5c \rightarrow KET-6 \rightarrow KET-7a \rightarrow HC-6.$$

This probable pathway is highlighted in Figure 6. Next, we look into the condensed phase effects on this more likely path to understand if the presence of a solvent causes differences.

4.2.3 Energetics in Liquid Phase

Table 8 summarizes the thermodynamics and kinetics of the important elementary surface processes for hydrogenation of phenol in various reaction environments. Presence of a solvent barely affects the thermodynamics or the kinetics of phenolate (KET-1) production from phenol (step 80) or the subsequent hydrogenation steps to form the KET-2b species (step 102) and KET-3g species (step 105). However, liquid water reduces the free energy of activation of the next hydrogenation step to produce KET-4d/b species (step 109) by 0.13 eV where the non-polar aprotic n-hexane demonstrates a less dramatic effect. Introduction of a liquid phase environment also facilitates the subsequent hydrogenation of KET-4b to KET-5c (step 92), with water displaying the largest facilitating effect ($\Delta(\Delta G_{water}^{\ddagger}) = -0.17\ eV$). KET-5c then undergoes hydrogenation to produce the KET-6 species (step 96) where condensed phases have a nominal effect on the thermodynamics of the reaction. However, the reaction becomes more facile in the liquid phase, with liquid water reducing the free energy of activation by 0.17 eV. The thermodynamics and kinetics of the final two subsequent hydrogenation steps (step 98 & 100) are minimally affected by the presence of a condensed phase. Overall, addition of a liquid phase reaction medium facilitates the likely pathway proposed in the previous section with liquid water exhibiting the largest facilitating effect which compares favorably with the experimental observation of Zhong et al.[92] However, the kinetics of some of these elementary processes (Table 8) still remains very demanding.

5. Conclusions

The solvent influence on the hydrodeoxygenation of guaiacol over a Ru(0001) model surface has been investigated by means of periodic DFT calculations, non-periodic implicit solvation calculations with iSMS scheme, and microkinetic modeling. In the first step, we examined the formation of unsaturated aromatic products such as phenol, anisole, catechol etc. from guaiacol. We developed mean-field microkinetic reactor models at different temperatures and experimental reaction conditions.[36,46] Under all reaction environments and reaction conditions, we found the same dominating HDO mechanism with the most favored pathway following the initial dehydrogenation at the hydroxyl group of guaiacol, followed by complete dehydrogenation of the methoxy group and subsequent decarbonylation, which then undergoes two subsequent hydrogenations to produce phenol. Less protic solvents such as 1-butanol, diethyl ether, and n-hexane demonstrate a higher HDO rate compared to that of vapor and aqueous phases which is qualitatively in good agreement with experimental results.[44] After verifying the presence of phenol, which is often referred to as a ‘short-lived intermediate’, we investigated the production of cycloalkanes through phenol hydrogenation in vapor and condensed phases. We observed that dehydrogenation of phenol to a phenolate species (keto-enol tautomerization pathway) is the most likely pathway to produce cyclohexanol and cyclohexanone from phenol. Based on the vapor phase first-principles calculations, we proposed a plausible pathway for cycloalkane formation. Next, we investigated the solvent effects on this probable reaction pathway and demonstrated a facilitating effect of an aqueous phase along the proposed reaction mechanism which is again in line with experimental observations.[98] Therefore, our study addresses a crucial issue, how the presence of a condensed phase affects the hydrogenation of aromatic rings over Ru catalysts. We note here that the proposed pathway still remains kinetically very challenging and it is possible that the cyclohexanone and cyclohexanol production follows a different reaction route along the keto-enol tautomerization pathway. Prior investigations have also shown that the support can play a major role in the hydrogenation of phenol which might also facilitate the kinetics of the reactions along the hypothesized reaction mechanism.[89] However, a full computational investigation of the phenol hydrogenation is out of the scope of the present study and we encourage further computational investigations on phenol hydrogenation for the production of cycloalkanes. Nevertheless, we can conclude that solvents with high degree of polarity are favorable for hydrogenation of the phenyl ring over Ru catalysts while non-polar solvents tend to facilitate the demethoxylation of guaiacol species.

Associated Content

Supporting Information

The Supporting Information is available free of charge on the ACS Publications website at DOI: XXX

Lateral interaction parameters employed in the microkinetic model, Kamlet and Taft solvatochromic parameters, free energies of elementary reaction at different temperatures, geometries of adsorbed intermediates and transition states.

Notes

The authors declare no competing financial interests.

Acknowledgements

We gratefully acknowledge the financial support of United States Department of Energy, Office of Basic Energy Sciences (DE-SC0007167). Computing resources provided by the National Energy Research Scientific Computing Center (NERSC), Texas Advanced Computing Center (TACC), and Pacific Northwest National Laboratory (PNNL) are gratefully acknowledged.

References

1. Li, Z.; Han, C.; Gu, T. Economics of biomass gasification: A review of the current status. *Energy Sources, Part B: Economics, Planning, and Policy* **2018,** *13*, 137-140.
2. Popp, J.; Lakner, Z.; Harangi-Rakos, M.; Fari, M. The effect of bioenergy expansion: Food, energy, and environment. *Renew Sust Energ Rev* **2014,** *32*, 559-578.
3. Carriquiry, M. A.; Du, X. D.; Timilsina, G. R. Second generation biofuels: Economics and policies. *Energ Policy* **2011,** *39*, 4222-4234.
4. Chheda, J. N.; Huber, G. W.; Dumesic, J. A. Liquid-phase catalytic processing of biomass-derived oxygenated hydrocarbons to fuels and chemicals. *Angewandte Chemie-International Edition* **2007,** *46*, 7164-7183.
5. Alonso, D. M.; Bond, J. Q.; Dumesic, J. A. Catalytic conversion of biomass to biofuels. *Green Chem* **2010,** *12*, 1493-1513.
6. Serrano-Ruiz, J. C.; Dumesic, J. A. Catalytic routes for the conversion of biomass into liquid hydrocarbon transportation fuels. *Energ Environ Sci* **2011,** *4*, 83-99.
7. Xiu, S. N.; Shahbazi, A. Bio-oil production and upgrading research: A review. *Renew Sust Energ Rev* **2012,** *16*, 4406-4414.
8. Furimsky, E. Catalytic hydrodeoxygenation. *Appl Catal a-Gen* **2000,** *199*, 147-190.
9. Honkela, M. L.; Viljava, T.-R.; Gutierrez, A.; Krause, A. O. I. In *Thermochemical Conversion of Biomass to Liquid Fuels and Chemicals*, The Royal Society of Chemistry, **2010**, pp. 288-306
10. Elliott, D. C.; Hart, T. R. Catalytic Hydroprocessing of Chemical Models for Bio-oil. *Energ Fuel* **2009,** *23*, 631-637.
11. Popov, A.; Kondratieva, E.; Mariey, L.; Goupil, J. M.; El Fallah, J.; Gilson, J. P.; Travert, A.; Mauge, F. Bio-oil hydrodeoxygenation: Adsorption of phenolic compounds on sulfided (Co)Mo catalysts. *J Catal* **2013,** *297*, 176-186.
12. Zhang, S. P.; Yan, Y. J.; Li, T. C.; Ren, Z. W. Upgrading of liquid fuel from the pyrolysis of biomass. *Bioresource Technol* **2005,** *96*, 545-550.
13. Wildschut, J.; Mahfud, F. H.; Venderbosch, R. H.; Heeres, H. J. Hydrotreatment of Fast Pyrolysis Oil Using Heterogeneous Noble-Metal Catalysts. *Ind Eng Chem Res* **2009,** *48*, 10324-10334.
14. Viljava, T. R.; Komulainen, S.; Selvam, T.; Krause, A. O. I. Stability of CoMo/Al2O3 catalysts: Effect of HDO cycles on HDS. *Stud Surf Sci Catal* **1999,** *127*, 145-152.
15. Viljava, T. R.; Komulainen, R. S.; Krause, A. O. I. Effect of H2S on the stability of CoMo/Al2O3 catalysts during hydrodeoxygenation. *Catal Today* **2000,** *60*, 83-92.
16. Gutierrez, A.; Kaila, R. K.; Honkela, M. L.; Slioor, R.; Krause, A. O. I. Hydrodeoxygenation of guaiacol on noble metal catalysts. *Catal Today* **2009,** *147*, 239-246.
17. Furimsky, E.; Massoth, F. Deactivation of hydroprocessing catalysts. *Catalysis Today* **1999,** *52*, 381-495.
18. Laurent, E.; Centeno, A.; Delmon, B. Coke Formation during the Hydrotreating of Biomass Pyrolysis Oils - Influence of Guaiacol Type Compounds. *Catalyst Deactivation 1994* **1994,** *88*, 573-578.
19. Laurent, E.; Delmon, B. Influence of Water in the Deactivation of a Sulfided Nimo Gamma-Al2o3 Catalyst during Hydrodeoxygenation. *J Catal* **1994,** *146*, 281-291.

20. Lin, Y. C.; Li, C. L.; Wan, H. P.; Lee, H. T.; Liu, C. F. Catalytic Hydrodeoxygenation of Guaiacol on Rh-Based and Sulfided CoMo and NiMo Catalysts. *Energ Fuel* **2011,** *25*, 890-896.

21. Mortensen, P. M.; Grunwaldt, J. D.; Jensen, P. A.; Knudsen, K. G.; Jensen, A. D. A review of catalytic upgrading of bio-oil to engine fuels. *Appl Catal a-Gen* **2011,** *407*, 1-19.

22. Holladay, J. E.; White, J. F.; Bozell, J. J.; Johnson, D. In *Top Value Added Chemicals from Biomass - Volume II, Results of Screening for Potential Candidates from Biorefinery Lignin*, Pacific Northwest National Lab., Richland, WA: 2007; pp 42-44.

23. Zakzeski, J.; Jongerius, A. L.; Bruijnincx, P. C. A.; Weckhuysen, B. M. Catalytic Lignin Valorization Process for the Production of Aromatic Chemicals and Hydrogen. *Chemsuschem* **2012,** *5*, 1602-1609.

24. Gonzalez-Borja, M. A.; Resasco, D. E. Anisole and Guaiacol Hydrodeoxygenation over Monolithic Pt-Sn Catalysts. *Energ Fuel* **2011,** *25*, 4155-4162.

25. Nimmanwudipong, T.; Runnebaum, R. C.; Block, D. E.; Gates, B. C. Catalytic Conversion of Guaiacol Catalyzed by Platinum Supported on Alumina: Reaction Network Including Hydrodeoxygenation Reactions. *Energ Fuel* **2011,** *25*, 3417-3427.

26. Lee, C. R.; Yoon, J. S.; Suh, Y. W.; Choi, J. W.; Ha, J. M.; Suh, D. J.; Park, Y. K. Catalytic roles of metals and supports on hydrodeoxygenation of lignin monomer guaiacol. *Catal Commun* **2012,** *17*, 54-58.

27. Nimmanwudipong, T.; Aydin, C.; Lu, J.; Runnebaum, R. C.; Brodwater, K. C.; Browning, N. D.; Block, D. E.; Gates, B. C. Selective Hydrodeoxygenation of Guaiacol Catalyzed by Platinum Supported on Magnesium Oxide. *Catal Lett* **2012,** *142*, 1190-1196.

28. Sun, J. M.; Karim, A. M.; Zhang, H.; Kovarik, L.; Li, X. H. S.; Hensley, A. J.; McEwen, J. S.; Wang, Y. Carbon-supported bimetallic Pd-Fe catalysts for vapor-phase hydrodeoxygenation of guaiacol. *J Catal* **2013,** *306*, 47-57.

29. He, Z.; Wang, X. Q. Highly selective catalytic hydrodeoxygenation of guaiacol to cyclohexane over Pt/TiO2 and NiMo/Al2O3 catalysts. *Front Chem Sci Eng* **2014,** *8*, 369-377.

30. Gao, D.; Schweitzer, C.; Hwang, H. T.; Varma, A. Conversion of Guaiacol on Noble Metal Catalysts: Reaction Performance and Deactivation Studies. *Ind Eng Chem Res* **2014,** *53*, 18658-18667.

31. Gao, D. N.; Xiao, Y.; Varma, A. Guaiacol Hydrodeoxygenation over Platinum Catalyst: Reaction Pathways and Kinetics. *Ind Eng Chem Res* **2015,** *54*, 10638-10644.

32. Lin, Y.-C.; Li, C.-L.; Wan, H.-P.; Lee, H.-T.; Liu, C.-F. Catalytic Hydrodeoxygenation of Guaiacol on Rh-Based and Sulfided CoMo and NiMo Catalysts. *Energy & Fuels* **2011,** *25*, 890-896.

33. Chang, J.; Danuthai, T.; Dewiyanti, S.; Wang, C.; Borgna, A. Hydrodeoxygenation of Guaiacol over Carbon-Supported Metal Catalysts. *Chemcatchem* **2013,** *5*, 3041-3049.

34. Hong, Y. K.; Lee, D. W.; Eom, H. J.; Lee, K. Y. The catalytic activity of Pd/WOx/gamma-Al2O3 for hydrodeoxygenation of guaiacol. *Appl Catal B-Environ* **2014,** *150*, 438-445.

35. Boonyasuwat, S.; Omotoso, T.; Resasco, D. E.; Crossley, S. P. Conversion of Guaiacol over Supported Ru Catalysts. *Catal Lett* **2013,** *143*, 783-791.

36. Nakagawa, Y.; Ishikawa, M.; Tamura, M.; Tomishige, K. Selective production of cyclohexanol and methanol from guaiacol over Ru catalyst combined with MgO. *Green Chem* **2014,** *16*, 2197-2203.

37. Olcese, R. N.; Bettahar, M.; Petitjean, D.; Malaman, B.; Giovanella, F.; Dufour, A. Gas-phase hydrodeoxygenation of guaiacol over Fe/SiO2 catalyst. *Applied Catalysis B: Environmental* **2012,** *115-116*, 63-73.

38. Bykova, M. V.; Ermakov, D. Y.; Kaichev, V. V.; Bulavchenko, O. A.; Saraev, A. A.; Lebedev, M. Y.; Yakovlev, V. A. Ni-based sol-gel catalysts as promising systems for crude bio-oil upgrading: Guaiacol hydrodeoxygenation study. *Appl Catal B-Environ* **2012,** *113*, 296-307.

39. Honkela, M. L.; Viljava, T. R.; Gutierrez, A.; Krause, A. O. I. Hydrotreating for Bio-Oil Upgrading. *Rsc Energy Environ S* **2010**, 288-306.

40. Schimming, S. M.; LaMont, O. D.; Konig, M.; Rogers, A. K.; D'Amico, A. D.; Yung, M. M.; Sievers, C. Hydrodeoxygenation of Guaiacol over Ceria-Zirconia Catalysts. *Chemsuschem* **2015,** *8*, 2073-2083.

41. Wildschut, J.; Mahfud, F.; Venderbosch, R.; Heeres, H. Hydrotreatment of Fast Pyrolysis Oil Using Heterogeneous Noble-Metal Catalysts. *Industrial & Engineering Chemistry Research* **2009,** *48*, 10324-10334.

42. Lu, J. M.; Heyden, A. Theoretical investigation of the reaction mechanism of the hydrodeoxygenation of guaiacol over a Ru(0001) model surface. *J Catal* **2015,** *321*, 39-50.

43. Narayan, S.; Muldoon, J.; Finn, M.; Fokin, V.; Kolb, H.; Sharpless, K. "On water": Unique reactivity of organic compounds in aqueous suspension. *Angewandte Chemie-International Edition* **2005,** *44*, 3275-3279.

44. Hellinger, M.; de Carvalho, H. W. P.; Baier, S.; Gharnati, L.; Grunwaldt, J. D. Solvent Influence on the Hydrodeoxygenation of Guaiacol over Pt/SiO2 and Pt/H-MFI90 Catalysts. *Chem-Ing-Tech* **2015,** *87*, 1771-1780.

45. Hellinger, M.; Baier, S.; Mortensen, P. M.; Kleist, W.; Jensen, A. D.; Grunwaldt, J. D. Continuous Catalytic Hydrodeoxygenation of Guaiacol over Pt/SiO2 and Pt/H-MFI-90. *Catalysts* **2015,** *5*, 1152-1166.

46. Ishikawa, M.; Tamura, M.; Nakagawa, Y.; Tomishige, K. Demethoxylation of guaiacol and methoxybenzenes over carbon-supported Ru-Mn catalyst. *Appl Catal B-Environ* **2016,** *182*, 193-203.

47. Reichardt, C.; Welton, T. In *Solvents and Solvent Effects in Organic Chemistry*, Reichardt, C.; Welton, T., Eds.; Wiley-VCH: Weinheim, Germany, **2011**; pp 425-508.

48. Faheem, M.; Suthirakun, S.; Heyden, A. New Implicit Solvation Scheme for Solid Surfaces. *J Phys Chem C* **2012,** *116*, 22458-22462.

49. Yoon, J. S.; Choi, J. W.; Suh, D. J.; Lee, K.; Lee, H.; Ha, J. M. Water-Assisted Selective Hydrodeoxygenation of Lignin-Derived Guaiacol to Monooxygenates. *Chemcatchem* **2015,** *7*, 2669-2674.

50. Saleheen, M.; Heyden, A. Liquid-Phase Modeling in Heterogeneous Catalysis. *Acs Catal* **2018,** *8*, 2188-2194.

51. Behtash, S.; Lu, J. M.; Faheem, M.; Heyden, A. Solvent effects on the hydrodeoxygenation of propanoic acid over Pd(111) model surfaces (vol 16, pg 605, 2014). *Green Chem* **2014,** *16*, 4427-4428.

52. Behtash, S.; Lu, J. M.; Walker, E.; Mamun, O.; Heyden, A. Solvent effects in the liquid phase hydrodeoxygenation of methyl propionate over a Pd(111) catalyst model. *J Catal* **2016,** *333*, 171-183.

53. Behtash, S.; Lu, J. M.; Mamun, O.; Williams, C. T.; Monnier, J. R.; Heyden, A. Solvation Effects in the Hydrodeoxygenation of Propanoic Acid over a Model Pd(211) Catalyst. *J Phys Chem C* **2016,** *120*, 2724-2736.

54. Mamun, O.; Saleheen, M.; Bond, J. Q.; Heyden, A. Importance of Angelica Lactone Formation in the Hydrodeoxygenation of Levulinic Acid to gamma-Valerolactone over a Ru(0001) Model Surface. *J Phys Chem C* **2017,** *121*, 18746-18761.

55. Klamt, A. Conductor-Like Screening Model for Real Solvents - a New Approach to the Quantitative Calculation of Solvation Phenomena. *J Phys Chem-Us* **1995,** *99*, 2224-2235.

56. Klamt, A. In *COSMO-RS: From Quantum Chemistry to Fluid Phase Thermodynamics and Drug Design*, 1st ed.; Elsevier Science Ltd.: Amsterdam, Netherlands, 2005.

57. Wellendorff, J.; Lundgaard, K. T.; Møgelhøj, A.; Petzold, V.; Landis, D. D.; Nørskov, J. K.; Bligaard, T.; Jacobsen, K. W. Density functionals for surface science: Exchange-correlation model development with Bayesian error estimation. *Phys Rev B* **2012,** *85*, 235149.

58. Wellendorff, J.; Silbaugh, T. L.; Garcia-Pintos, D.; Norskov, J. K.; Bligaard, T.; Studt, F.; Campbell, C. T. A benchmark database for adsorption bond energies to transition metal surfaces and comparison to selected DFT functionals. *Surf Sci* **2015,** *640*, 36-44.

59. Liu, W.; Tkatchenko, A.; Scheffler, M. Modeling Adsorption and Reactions of Organic Molecules at Metal Surfaces. *Accounts of Chemical Research* **2014,** *47*, 3369-3377.

60. Studt, F.; Abild-Pedersen, F.; Varley, J. B.; Norskov, J. K. CO and CO2 Hydrogenation to Methanol Calculated Using the BEEF-vdW Functional. *Catal Lett* **2013,** *143*, 71-73.

61. Studt, F.; Behrens, M.; Kunkes, E. L.; Thomas, N.; Zander, S.; Tarasov, A.; Schumann, J.; Frei, E.; Varley, J. B.; Abild-Pedersen, F.; Norskov, J. K.; Schlogl, R. The Mechanism of CO and CO2 Hydrogenation to Methanol over Cu-Based Catalysts. *Chemcatchem* **2015,** *7*, 1105-1111.

62. Perdew, J. P.; Burke, K.; Ernzerhof, M. Generalized gradient approximation made simple. *Phys Rev Lett* **1996,** *77*, 3865-3868.

63. Grimme, S.; Antony, J.; Ehrlich, S.; Krieg, H. A consistent and accurate ab initio parametrization of density functional dispersion correction (DFT-D) for the 94 elements H-Pu. *J Chem Phys* **2010,** *132*.

64. Ahlrichs, R.; Bar, M.; Haser, M.; Horn, H.; Kolmel, C. Electronic-Structure Calculations on Workstation Computers - the Program System Turbomole. *Chem Phys Lett* **1989,** *162*, 165-169.

65. Von Arnim, M.; Ahlrichs, R. Performance of parallel TURBOMOLE for density functional calculations. *J Comput Chem* **1998,** *19*, 1746-1757.

66. Weigend, F.; Ahlrichs, R. Balanced basis sets of split valence, triple zeta valence and quadruple zeta valence quality for H to Rn: Design and assessment of accuracy. *Phys Chem Chem Phys* **2005,** *7*, 3297-3305.

67. Russo, T. V.; Martin, R. L.; Hay, P. J. Effective Core Potentials for Dft Calculations. *J Phys Chem-Us* **1995,** *99*, 17085-17087.

68. Becke, A. D. Density-Functional Exchange-Energy Approximation with Correct Asymptotic-Behavior. *Phys Rev A* **1988,** *38*, 3098-3100.

69. Perdew, J. P. Density-Functional Approximation for the Correlation-Energy of the Inhomogeneous Electron-Gas. *Phys Rev B* **1986,** *33*, 8822-8824.

70. Eichkorn, K.; Treutler, O.; Ohm, H.; Haser, M.; Ahlrichs, R. Auxiliary Basis-Sets to Approximate Coulomb Potentials. *Chem Phys Lett* **1995,** *240*, 283-289.

71. Weigend, F. Accurate Coulomb-fitting basis sets for H to Rn. *Phys Chem Chem Phys* **2006,** *8*, 1057-1065.

72. Eichkorn, K.; Weigend, F.; Treutler, O.; Ahlrichs, R. Auxiliary basis sets for main row atoms and transition metals and their use to approximate Coulomb potentials. *Theor Chem Acc* **1997,** *97*, 119-124.

73. Klamt, A.; Schuurmann, G. Cosmo - a New Approach to Dielectric Screening in Solvents with Explicit Expressions for the Screening Energy and Its Gradient. *J Chem Soc, Perkin Trans 2* **1993**, 799-805.

74. Schafer, A.; Klamt, A.; Sattel, D.; Lohrenz, J. C. W.; Eckert, F. COSMO Implementation in TURBOMOLE: Extension of an efficient quantum chemical code towards liquid systems. *Phys Chem Chem Phys* **2000,** *2*, 2187-2193.

75. Faheem, M.; Saleheen, M.; Lu, J. M.; Heyden, A. Ethylene glycol reforming on Pt(111): first-principles microkinetic modeling in vapor and aqueous phases. *Catal Sci Technol* **2016,** *6*, 8242-8256. **A new transition state for primary C-H cleavage of ethylene glycol was later found which has 0.10 eV lower energy than reported herein.*

76. Chen, W.; Luo, Z. Y.; Yu, C. J.; Yang, Y.; Li, G. X.; Zhang, J. X. Catalytic conversion of guaiacol in ethanol for bio-oil upgrading to stable oxygenated organics. *Fuel Process Technol* **2014,** *126*, 420-428.

77. Lu, M. H.; Du, H.; Wei, B.; Zhu, J.; Li, M. S.; Shan, Y. H.; Shen, J. Y.; Song, C. S. Hydrodeoxygenation of Guaiacol on Ru Catalysts: Influence of TiO2-ZrO2 Composite Oxide Supports. *Ind Eng Chem Res* **2017,** *56*, 12070-12079.

78. Zhao, C.; He, J. Y.; Lemonidou, A. A.; Li, X. B.; Lercher, J. A. Aqueous-phase hydrodeoxygenation of bio-derived phenols to cycloalkanes. *J Catal* **2011,** *280*, 8-16.

79. Kamlet, M. J.; Taft, R. W. Solvatochromic Comparison Method .1. Beta-Scale of Solvent Hydrogen-Bond Acceptor (Hba) Basicities. *J Am Chem Soc* **1976,** *98*, 377-383.

80. Yokoyama, T.; Taft, R. W.; Kamlet, M. J. Solvatochromic Comparison Method .3. Hydrogen-Bonding by Some 2-Nitroaniline Derivatives. *J Am Chem Soc* **1976,** *98*, 3233-3237.

81. Taft, R. W.; Kamlet, M. J. Solvatochromic Comparison Method .2. Alpha-Scale of Solvent Hydrogen-Bond Donor (Hbd) Acidities. *J Am Chem Soc* **1976,** *98*, 2886-2894.

82. Mcquarrie, D. A. In *Statistical Mechanics,* 1st ed.; Harper and Row, New York, **1976,** pp. 21-141.

83. Pechukas, P. Transition-State Theory. *Annu Rev Phys Chem* **1981,** *32*, 159-177.

84. Kandoi, S.; Greeley, J.; Sanchez-Castillo, M. A.; Evans, S. T.; Gokhale, A. A.; Dumesic, J. A.; Mavrikakis, M. Prediction of experimental methanol decomposition rates on platinum from first principles. *Top Catal* **2006,** *37*, 17-28.

85. Mamun, O.; Walker, E.; Faheem, M.; Bond, J. Q.; Heyden, A. Theoretical Investigation of the Hydrodeoxygenation of Levulinic Acid to gamma-Valerolactone over Ru(0001). *Acs Catal* **2017,** *7*, 215-228.

86. Getman, R. B.; Schneider, W. F. DFT-based characterization of the multiple adsorption modes of nitrogen oxides on Pt(111). *J Phys Chem C* **2007,** *111*, 389-397.

87. Xu, Y.; Getman, R. B.; Shelton, W.; Schneider, W. F. A first-principles investigation of the effect of Pt cluster size on CO and NO oxidation intermediates and energetics. *Phys Chem Chem Phys* **2008,** *39,* 6009-6018.

88. Grabow, L. C.; Hvolbaek, B.; Norskov, J. K. Understanding Trends in Catalytic Activity: The Effect of Adsorbate-Adsorbate Interactions for CO Oxidation Over Transition Metals. *Top Catal* **2010,** *53*, 298-310.

89. Wang, Y.; Yao, J.; Li, H. R.; Su, D. S.; Antonietti, M. Highly Selective Hydrogenation of Phenol and Derivatives over a Pd@Carbon Nitride Catalyst in Aqueous Media. *J Am Chem Soc* **2011,** *133*, 2362-2365.

90. He, J.; Lu, X. H.; Shen, Y.; Jing, R.; Nie, R. F.; Zhou, D.; Xia, Q. H. Highly selective hydrogenation of phenol to cyclohexanol over nano silica supported Ni catalysts in aqueous medium. *Mol Catal* **2017,** *440*, 87-95.

91. Giraldo, L.; Bastidas-Barranco, M.; Moreno-Pirajan, J. C. Vapour Phase Hydrogenation of Phenol over Rhodium on SBA-15 and SBA-16. *Molecules* **2014,** *19*, 20594-20612.

92. Liu, H. Z.; Jiang, T.; Han, B. X.; Liang, S. G.; Zhou, Y. X. Selective Phenol Hydrogenation to Cyclohexanone Over a Dual Supported Pd-Lewis Acid Catalyst. *Science* **2009,** *326*, 1250-1252.

93. He, J. Y.; Zhao, C.; Lercher, J. A. Impact of solvent for individual steps of phenol hydrodeoxygenation with Pd/C and HZSM-5 as catalysts. *J Catal* **2014,** *309*, 362-375.

94. Campbell, C. T. Micro- and macro-kinetics: their relationship in heterogeneous catalysis. *Top Catal* **1994,** *1*, 353-366.

95. Campbell, C. T. Finding the rate-determining step in a mechanism - Comparing DeDonder relations with the "degree of rate control". *J Catal* **2001,** *204*, 520-524.

96. Stegelmann, C.; Andreasen, A.; Campbell, C. T. Degree of Rate Control: How Much the Energies of Intermediates and Transition States Control Rates. *J Am Chem Soc* **2009,** *131*, 8077-8082.

97. Evans, M. G.; Polanyi, M. Further considerations on the thermodynamics of chemical equilibria and reaction rates. *T Faraday Soc* **1936,** *32*, 1333-1359.

98. Zhong, J. W.; Chen, J. Z.; Chen, L. M. Selective hydrogenation of phenol and related derivatives. *Catal Sci Technol* **2014,** *4*, 3555-3569.

99. Kresse, G.; Hafner, J. *Ab initio* molecular dynamics for liquid metals. *Phys. Rev. B: Condens. Matter Mater. Phys.* **1993**, 47, 558−561.

100. Tshepelevitsh, S.; Oss, M.; Pung, A.; Leito, I. Evaluating the COSMO-RS Method for Modeling Hydrogen Bonding in Solution. *ChemPhysChem* 2013, 14, 1909-1919.

101. Saleheen, M.; Zare, M.; Faheem, M.; Heyden, A. Computational Investigation of Aqueous Phase Effects on the Dehydrogenation and Dehydroxylation of Polyols over Pt(111) *J Phys Chem C* **2019** *123* (31), 19052-19065

Table 1. Solvent effects on the adsorption strength of various surface intermediates in the HDO of guaiacol over a Ru(0001) model surface at 473 K.

Surface Intermediates	Water Δ(ΔG) (eV)	1-Butanol Δ(ΔG) (eV)	Diethyl ether Δ(ΔG) (eV)	n-Hexane Δ(ΔG) (eV)
$C_6H_4(OH)(OCH_3)$	-0.22	-0.47	-0.43	-0.33
$C_6H_4H_\beta(OH)(OCH_3)$	-0.18	-0.36	-0.34	-0.25
$C_6H_4H_\alpha(OH)(OCH_3)$	-0.19	-0.53	-0.50	-0.39
$C_6H_4OCH_3$	-0.07	-0.35	-0.33	-0.24
C_6H_4OH	-0.20	-0.33	-0.31	-0.22
$C_6H_4(OH)(OCH_2)$	-0.15	-0.43	-0.40	-0.30
$C_6H_4(OH)(O)$	-0.22	-0.26	-0.23	-0.15
$C_6H_4(O)(OCH_3)$	-0.16	-0.35	-0.31	-0.22
$C_6H_4H_\beta(OH)(OCH_2)$	-0.37	-0.38	-0.35	-0.26
$C_6H_5OCH_3$	-0.25	-0.41	-0.38	-0.29
$C_6H_4(OH)(OCH)$	-0.17	-0.44	-0.41	-0.30
$C_6H_4(OH)_2$	-0.22	-0.39	-0.36	-0.25
C_6H_4O	-0.05	-0.33	-0.31	-0.22
$C_6H_4(O)(OCH_2)$	-0.14	-0.29	-0.25	-0.17
$C_6H_4H_\beta(OH)(O)$	-0.19	-0.33	-0.29	-0.20
$C_6H_5OCH_2$	-0.17	-0.32	-0.28	-0.19
C_6H_5O	-0.13	-0.32	-0.29	-0.20
C_6H_5OH	-0.20	-0.38	-0.35	-0.26
$C_6H_5(OH)_2$	-0.14	-0.28	-0.25	-0.18
$C_6H_4O_2$	-0.26	-0.34	-0.31	-0.23
C_6H_5	-0.14	-0.31	-0.29	-0.21
C_6H_6OH	-0.22	-0.28	-0.25	-0.17
C_6H_6	-0.11	-0.26	-0.24	-0.17
$C_6H_4H\alpha(O)(OH)$	-0.19	-0.27	-0.24	-0.17
$C_6H_4(O)(OCH)$	-0.18	-0.34	-0.32	-0.24
$C_6H_4(O)(OC)$	-0.27	-0.32	-0.29	-0.20
H	0.04	0.01	0.01	0.01
OH	0.04	-0.02	-0.02	0.01
H_2O	0.01	-0.10	-0.09	-0.05
CH	-0.05	-0.02	-0.01	0.01
CH_2	0.02	-0.02	-0.01	0.00
CH_3	0.11	-0.01	-0.01	0.00
CH_4	0.04	-0.03	-0.03	-0.03
CO	0.00	-0.06	-0.06	-0.04
CHO	0.02	-0.04	-0.04	-0.01
CH_2O	-0.02	-0.03	-0.02	0.00
CH_3O	0.09	-0.07	-0.06	-0.04
CH_3OH	0.12	-0.10	-0.09	-0.05

Table 2: Energetics of adsorption-desorption reactions (in eV) for the HDO of guaiacol in the limit of zero coverage at 473 K temperature under different reaction environments.

ID	Reaction	Vapor phase, ΔG_{rxn}	Water, ΔG_{rxn}	1-Butanol, ΔG_{rxn}	Diethyl ether, ΔG_{rxn}	n-Hexane, ΔG_{rxn}
1	$C_6H_4(OH)(OCH_3)$ (gas) + 4* ↔ $C_6H_4(OH)(OCH_3)$ ****	-0.29	-0.51	-0.75	-0.72	-0.62
53	$C_6H_5(OCH_3)$**** ↔ $C_6H_5(OCH_3)$ (gas) + 4*	0.35	0.60	0.75	0.73	0.64
54	$C_6H_4(OH)_2$**** ↔ $C_6H_4(OH)_2$(gas) + 4*	0.41	0.63	0.80	0.77	0.66
55	C_6H_5OH**** ↔ C_6H_5OH (gas) + 4*	0.45	0.65	0.83	0.80	0.71
56	C_6H_6*** ↔ C_6H_6(gas) + 3*	0.47	0.58	0.72	0.70	0.64
57	CH_4* ↔ CH_4(gas) + *	-0.39	-0.43	-0.36	-0.36	-0.36
58	CH_3OH* ↔ CH_3OH (gas) + *	-0.38	-0.50	-0.28	-0.29	-0.33
59	H_2O* ↔ H_2O (gas) + *	-0.33	-0.34	-0.23	-0.24	-0.28
60	CO* ↔ CO (gas) + *	0.96	0.96	1.02	1.01	1.00
53	H* ↔ $0.5H_2$ (gas) + *	0.18	0.22	0.19	0.19	0.19

Table 3. Energetics of all elementary surface reaction steps (in eV) for the HDO of guaiacol to aromatics in the limit of zero coverage at 473 K in the presence of liquid water, 1-butanol, diethyl ether, and n-hexane solvents.

ID	Reaction	Vapor phase		Water		1-Burtanol		Diethyl ether		n-Hexane	
		ΔG_{rxn}	$\Delta G^{\ddagger}$	ΔG_{rxn}	$\Delta G^{\ddagger}$	ΔG_{rxn}	$\Delta G^{\ddagger}$	ΔG_{rxn}	$\Delta G^{\ddagger}$	ΔG_{rxn}	$\Delta G^{\ddagger}$
2	$C_6H_4(OH)(OCH_3)**** + H* \leftrightarrow C_6H_4H_\beta(OH)(OCH_3)**** + *$	0.40	1.10	0.41	1.12	0.49	1.27	0.48	1.28	0.47	1.25
3	$C_6H_4(OH)(OCH_3)\ **** + H* \leftrightarrow C_6H_4H_\alpha(OH)(OCH_3)**** + *$	0.51	1.14	0.51	1.18	0.43	1.20	0.44	1.20	0.45	1.21
4	$C_6H_4(OH)(OCH_3)**** + * \leftrightarrow C_6H_4(OCH_3)**** + OH*$	-0.22	1.06	-0.03	1.13	-0.13	1.06	-0.13	1.06	-0.12	1.07
5	$C_6H_4(OH)(OCH_3)**** + * \leftrightarrow C_6H_4OH**** + CH_3O*$	-0.49	0.88	-0.37	0.95	-0.43	0.89	-0.42	0.90	-0.42	0.90
6	$C_6H_4(OH)(OCH_3)**** + 2* \leftrightarrow C_6H_4(OH)(OCH_2)***** + H*$	-0.36	0.50	-0.25	0.52	-0.32	0.51	-0.32	0.51	-0.32	0.51
7	$C_6H_4(OH)(OCH_3)**** + * \leftrightarrow C_6H_4(OH)(O)**** + CH_3*$	-1.35	1.40	-1.23	1.43	-1.15	1.36	-1.15	1.37	-1.17	1.38
8	$C_6H_4(OH)(OCH_3)**** + * \leftrightarrow C_6H_4(O)(OCH_3)**** + H*$	-0.77	0.29	-0.67	0.37	-0.65	0.29	-0.64	0.29	-0.65	0.31
9	$C_6H_4H_\beta(OH)(OCH_3)**** + 2* \leftrightarrow C_6H_4H_\beta(OH)(OCH_2)***** + H*$	-0.12	0.93	-0.27	0.81	-0.13	0.91	-0.12	0.92	-0.12	0.93
10	$C_6H_4H_\beta(OH)(OCH_3)**** + * \leftrightarrow C_6H_5OH**** + CH_3O*$	-1.05	0.72	-0.97	0.61	-1.13	0.66	-1.12	0.67	-1.10	0.68
11	$C_6H_4H_\alpha(OH)(OCH_3)**** + * \leftrightarrow C_6H_5(OCH_3)**** + OH*$	-0.91	0.57	-0.93	0.59	-0.81	0.70	-0.81	0.70	-0.81	0.68
12	$C_6H_4(OCH_3)**** + H* \leftrightarrow C_6H_5(OCH_3)**** + *$	-0.18	0.64	-0.40	0.58	-0.25	0.55	-0.25	0.55	-0.24	0.56
13	$C_6H_4OH**** + H* \leftrightarrow C_6H_5OH**** + *$	-0.16	0.62	-0.20	0.59	-0.22	0.61	-0.21	0.61	-0.21	0.60
14	$C_6H_4(OH)(OCH_2)***** + * \leftrightarrow C_6H_4OH**** + CH_2O**$	-0.25	1.23	-0.33	1.10	-0.19	1.34	-0.19	1.33	-0.18	1.32
15	$C_6H_4(OH)(OCH_2)***** + * \leftrightarrow C_6H_4(O)(OCH_2)***** + H*$	-0.73	0.28	-0.69	0.31	-0.58	0.32	-0.58	0.32	-0.59	0.31
16	$C_6H_4(OH)(OCH_2)***** + * \leftrightarrow C_6H_4(OH)(OCH)***** + H*$	-0.53	0.02	-0.52	0.00	-0.53	0.12	-0.53	0.12	-0.53	0.11
17	$C_6H_4(OH)(OCH_2)***** \leftrightarrow C_6H_4(OH)(O)**** + CH_2*$	-1.25	0.42	-1.30	0.43	-1.10	0.40	-1.10	0.40	-1.11	0.41
18	$C_6H_4(OH)(O)**** + H* \leftrightarrow C_6H_4(OH)_2**** + *$	0.75	1.03	0.71	1.03	0.61	0.92	0.61	0.92	0.64	0.93
19	$C_6H_4(OH)(O)**** + H* \leftrightarrow C_6H_4H_\alpha(OH)(O)**** + *$	0.89	1.40	0.87	1.47	0.86	1.37	0.86	1.37	0.85	1.38
20	$C_6H_4(OH)(O)**** + * \leftrightarrow C_6H_4O**** + OH*$	0.51	1.15	0.72	1.11	0.41	1.14	0.42	1.14	0.45	1.15
21	$C_6H_4(O)(OCH_3)**** + * \leftrightarrow C_6H_4O**** + CH_3O*$	0.21	1.08	0.32	1.04	0.16	1.15	0.17	1.16	0.19	1.16
22	$C_6H_4(O)(OCH_3)**** + 2* \leftrightarrow C_6H_4(O)(OCH_2)***** + H*$	-0.32	0.53	-0.27	0.47	-0.25	0.52	-0.25	0.51	-0.26	0.51
23	$C_6H_4H_\beta(OH)(OCH_2)***** \leftrightarrow C_6H_4H_\beta(OH)(O)**** + CH_2*$	-0.84	0.39	-0.65	0.55	-0.81	0.39	-0.80	0.40	-0.79	0.41
24	$C_6H_5(OCH_3)**** + * \leftrightarrow C_6H_5(OCH_2)**** + H*$	-0.32	0.51	-0.20	0.52	-0.22	0.55	-0.21	0.56	-0.21	0.57

25	$C_6H_4(OH)(OCH)$***** + * ↔ C_6H_4OH**** + CHO**	-0.26	1.00	-0.27	0.99	-0.20	0.95	-0.20	0.95	-0.20	0.95
26	$C_6H_4(OH)(OCH)$***** ↔ $C_6H_4(OH)(O)$**** + CH*	-1.29	0.31	-1.38	0.31	-1.12	0.32	-1.12	0.33	-1.13	0.34
27	$C_6H_4(OH)_2$**** + * ↔ C_6H_4OH**** + OH*	-0.16	1.16	-0.09	1.09	-0.13	1.16	-0.13	1.16	-0.13	1.15
28	$C_6H_4(OH)_2$**** + H* ↔ $C_6H_5(OH)_2$**** + *	0.55	1.15	0.59	1.25	0.65	1.19	0.65	1.19	0.62	1.17
29	$C_6H_4H_\alpha(OH)(O)$**** + * ↔ C_6H_5O**** + OH*	-1.29	0.76	-1.20	0.74	-1.37	0.73	-1.36	0.73	-1.31	0.74
30	C_6H_4O**** + H* ↔ C_6H_5O**** + *	-0.92	0.52	-1.04	0.43	-0.92	0.44	-0.91	0.45	-0.91	0.46
31	$C_6H_4(O)(OCH_2)$***** + * ↔ C_6H_4O**** + CH_2O**	0.40	1.03	0.46	1.01	0.32	1.02	0.32	1.02	0.34	1.01
32	$C_6H_4(O)(OCH_2)$***** + * ↔ $C_6H_4O_2$***** + CH_2*	-0.95	0.52	-1.05	0.50	-1.02	0.51	-1.02	0.51	-1.01	0.50
33	$C_6H_4(O)(OCH_2)$***** + * ↔ $C_6H_4(O)(OCH)$***** + H*	-0.52	0.02	-0.52	0.02	-0.57	0.00	-0.57	0.00	-0.58	0.00
34	$C_6H_4(O)(OCH)$***** + * ↔ $C_6H_4O_2$***** + CH*	-1.00	0.50	-1.13	0.52	-1.02	0.51	-1.01	0.53	-0.98	0.54
35	$C_6H_4(O)(OCH)$***** + * ↔ $C_6H_4(O)(OC)$***** + H*	-0.34	0.40	-0.39	0.41	-0.31	0.45	-0.30	0.46	-0.29	0.47
36	$C_6H_4H_\beta(OH)(O)$**** + H* ↔ $C_6H_5(OH)_2$**** + *	0.25	0.91	0.26	0.94	0.29	0.92	0.28	0.92	0.27	0.92
37	$C_6H_5(OCH_2)$**** + * ↔ C_6H_5O**** + CH_2*	-1.30	0.18	-1.24	0.16	-1.32	0.24	-1.32	0.23	-1.31	0.23
38	C_6H_5O**** + H* ↔ C_6H_5OH**** + *	0.84	1.03	0.73	1.00	0.77	1.04	0.76	1.04	0.77	1.03
39	C_6H_5OH**** + * ↔ C_6H_5**** + OH*	-0.10	1.17	-0.01	1.09	-0.07	1.21	-0.06	1.21	-0.05	1.20
40	C_6H_5OH**** + H* ↔ C_6H_6OH**** + *	0.59	1.25	0.53	1.21	0.67	1.34	0.67	1.34	0.67	1.33
41	$C_6H_5(OH)_2$**** + * ↔ C_6H_5OH**** + OH*	-0.87	0.56	-0.89	0.57	-0.99	0.41	-0.99	0.41	-0.95	0.45
42	$C_6H_4O_2$***** + H* ↔ $C_6H_4(OH)(O)$**** + 2*	0.43	0.95	0.44	0.97	0.50	0.95	0.51	0.95	0.50	0.95
43	$C_6H_4(O)(OC)$***** ↔ C_6H_4O**** + CO*	-0.49	0.66	-0.28	0.70	-0.57	0.69	-0.57	0.70	-0.55	0.69
44	C_6H_5**** + H* ↔ C_6H_6*** + 2*	-0.20	0.54	-0.21	0.56	-0.15	0.53	-0.15	0.54	-0.17	0.55
45	C_6H_6OH**** ↔ C_6H_6*** + OH*	-0.89	0.53	-0.74	0.59	-0.88	0.55	-0.89	0.54	-0.88	0.54
46	CH* + H* ↔ CH_2* + *	0.57	0.61	0.60	0.60	0.56	0.56	0.56	0.56	0.56	0.57
47	CH_2* + H* ↔ CH_3* + *	0.27	0.62	0.31	0.61	0.26	0.57	0.26	0.58	0.26	0.58
48	CH_3* + H* ↔ CH_4* + *	0.43	1.03	0.32	1.08	0.40	0.98	0.39	0.99	0.40	1.00
49	OH* + H* ↔ H_2O* + *	0.48	1.13	0.41	1.04	0.39	1.11	0.40	1.11	0.42	1.12
50	CHO** + H* ↔ CH_2O** + *	0.54	0.51	0.46	0.48	0.54	0.50	0.55	0.50	0.54	0.50
51	CH_2O** + H* ↔ CH_3O* + 2*	0.13	0.69	0.21	0.71	0.08	0.68	0.08	0.67	0.08	0.67
52	CH_3O* + H* ↔ CH_3OH* + *	0.71	1.21	0.69	1.16	0.67	1.23	0.67	1.23	0.69	1.23

Table 4: Computed overall turnover frequencies at various reaction temperatures and 15 bar partial pressure of hydrogen for the HDO of guaiacol over a Ru(0001) surface. Microkinetic models have been simulated for 1% conversion of guaiacol using 0.5 g guaiacol in 10 g of various solvent media. For vapor phase simulations, we used a guaiacol chemical potential corresponding to the one in liquid water.

TOF (s^{-1})	Temperature			
	423 K	473 K	523 K	573 K
Vapor phase	6.46×10^{-7}	1.95×10^{-4}	4.31×10^{-2}	2.35
Water	1.54×10^{-7}	6.70×10^{-5}	3.25×10^{-2}	4.82×10^{-1}
1-Butanol	4.64×10^{-6}	4.66×10^{-4}	1.76×10^{-2}	3.08×10^{-1}
Diethyl ether	4.07×10^{-6}	4.33×10^{-4}	1.80×10^{-2}	2.98×10^{-1}
n-Hexane	4.94×10^{-6}	5.17×10^{-4}	2.34×10^{-2}	4.14×10^{-1}

Table 5. Coverages (%) of most abundant surface intermediates in various reaction environments for the HDO of guaiacol at 473K.

Surface Intermediates	Vapor phase	Water	1-Butanol	Diethyl ether	n-Hexane
θ^*	0.13	0.10	0.39	0.41	0.35
θ^*_{H}	7.04	11.73	11.42	11.49	11.03
θ^*_{CO}	28.17	25.78	29.96	30.09	29.65
θ^*_{CH}	62.75	60.20	0.03	0.05	0.34
θ^*_{C6H4O2}	0.65	0.10	46.7	48.45	51.20
$\theta^*_{Phenoxy}$	0.76	1.84	9.72	8.24	5.68

Table 6. Kinetic parameters computed at 473 K for the HDO of guaiacol over a Ru(0001) model surface at low conversion conditions in various reaction environments.

Properties	Partial pressure (bar)	Vapor phase	Water	1-Butanol	Diethyl ether	n-Hexane
Apparent Activation Energy(eV)	-	2.12	2.15	1.55	1.57	1.58
Guaiacol order	0.20 - 10.0	0.17	0.20	0.12	0.12	0.12
Carbon monoxide order	1.0×10^{-5}-1.0×10^{-1}	-0.51	-0.65	-0.18	-0.18	-0.18
Hydrogen order	0.20 – 0.40	-1.18	-4.02	0.68	0.59	0.43
	0.60-20.0	1.74	1.62	0.46	0.46	0.44

Table 7. Thermodynamic and kinetic sensitivity analysis at 473 K for the HDO of guaiacol over a Ru(0001) model surface.

Degree of thermodynamic rate control					
Species	Vapor	Water	1-Butanol	Diethyl ether	n-Hexane
H*	-0.94	-0.35	-0.60	-0.66	-0.55
CO*	-0.63	-0.79	-0.18	-0.20	-0.21
CH*	-0.90	-0.86	0.00	0.00	0.00
$C_6H_4O_2$*****	-0.01	0.00	-0.80	-0.82	-0.82
Degree of kinetic rate control					
$C_6H_4(OH)(OCH_3)$ (gas) + 4* ↔ $C_6H_4(OH)(OCH_3)$****	0.15	0.20	0.16	0.16	0.16
$C_6H_4(OH)(O)$**** + * ↔ C_6H_4O**** + OH*	-0.01	0.01	0.77	0.80	0.82
$C_6H_4(O)(OCH)$***** + * ↔ $C_6H_4O_2$***** + CH*	-0.72	-0.75	-0.60	-0.61	-0.64
$C_6H_4(O)(OCH)$***** + * ↔ $C_6H_4(O)(OC)$***** + H*	0.74	0.73	0.57	0.58	0.61
CH_3* + H* ↔ CH_4* + *	0.84	0.86	0.00	0.00	0.01

Table 8. Energetics of important elementary surface reaction steps (in eV) in the limit of zero coverage at 473 K in the presence of liquid water, 1-butanol, diethyl ether, and n-hexane solvents for the phenol hydrogenation to cyclohexanol. Condensed phase effects have not been computed for reactions 1, 37, 52, and 77 due to their high activation barriers in vapor phase in comparison to the alternate route reaction 80.

ID	Reaction	Vapor phase		Water		1-Burtanol		Diethyl ether		n-Hexane	
		ΔG_{rxn}	$\Delta G^{\ddagger}$	ΔG_{rxn}	$\Delta G^{\ddagger}$	ΔG_{rxn}	$\Delta G^{\ddagger}$	ΔG_{rxn}	$\Delta G^{\ddagger}$	ΔG_{rxn}	$\Delta G^{\ddagger}$
1	Phenol**** + H* ↔ HC1-1**** + *	0.41	1.16	N/A	N/A	N/A	N/A	N/A	N/A	N/A	N/A
37	Phenol**** + H* ↔ HC2-1**** + *	0.58	1.11	N/A	N/A	N/A	N/A	N/A	N/A	N/A	N/A
52	Phenol**** + H* ↔ HC3-1**** + *	0.51	1.05	N/A	N/A	N/A	N/A	N/A	N/A	N/A	N/A
77	Phenol**** + H* ↔ HC4-1**** + *	0.71	1.15	N/A	N/A	N/A	N/A	N/A	N/A	N/A	N/A
80	Phenol**** + * ↔ KET-1**** + H*	-0.76	0.31	-0.77	0.34	-0.75	0.32	-0.75	0.32	-0.75	0.31
92	KET-4b**** + H* ↔ KET-5c**** + *	0.17	1.07	0.12	0.90	0.10	0.97	0.10	0.98	0.10	0.99
96	KET-5c**** + H* ↔ KET-6**** + *	0.32	1.21	0.23	1.04	0.24	1.15	0.24	1.17	0.24	1.18
98	KET-6**** + H* ↔ KET-7a**** + *	0.60	1.22	0.57	1.17	0.59	1.24	0.59	1.25	0.59	1.26
100	KET-7a**** + H* ↔ HC-6**** + *	-0.11	1.17	-0.13	1.09	-0.14	1.10	-0.13	1.11	-0.13	1.11
102	KET-1**** + H* ↔ KET-2b**** + *	0.94	1.14	0.90	1.21	0.90	1.14	0.90	1.13	0.90	1.12
105	KET-2b**** + H* ↔ KET-3g**** + *	0.27	0.84	0.24	0.86	0.23	0.81	0.23	0.80	0.23	0.80
109	KET-3g**** + H* ↔ KET-4d**** (=KET-4b****) + *	0.42	1.06	0.44	0.93	0.44	0.95	0.44	0.96	0.43	1.02

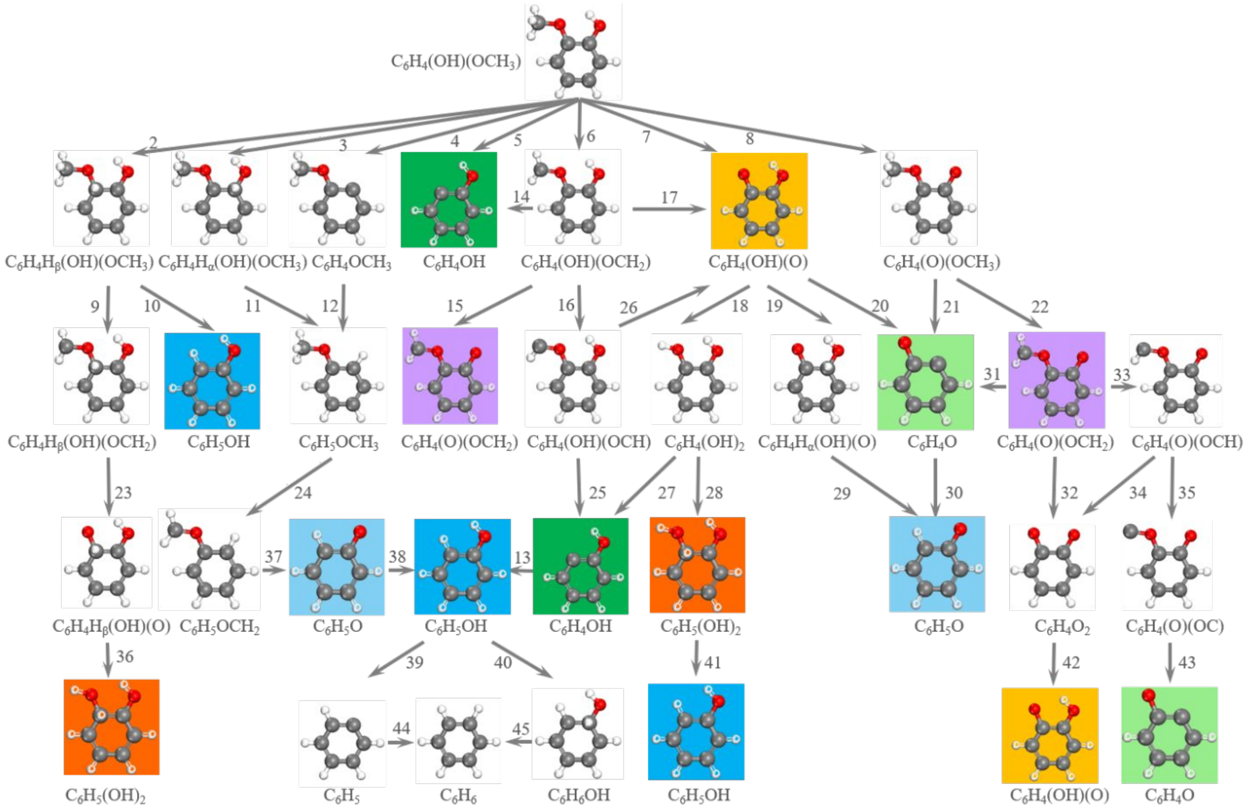

Figure 1: Reaction network investigated for the hydrodeoxygenation of guaiacol over a Ru(0001) model surface. Duplicate structures are highlighted by identical background colors.

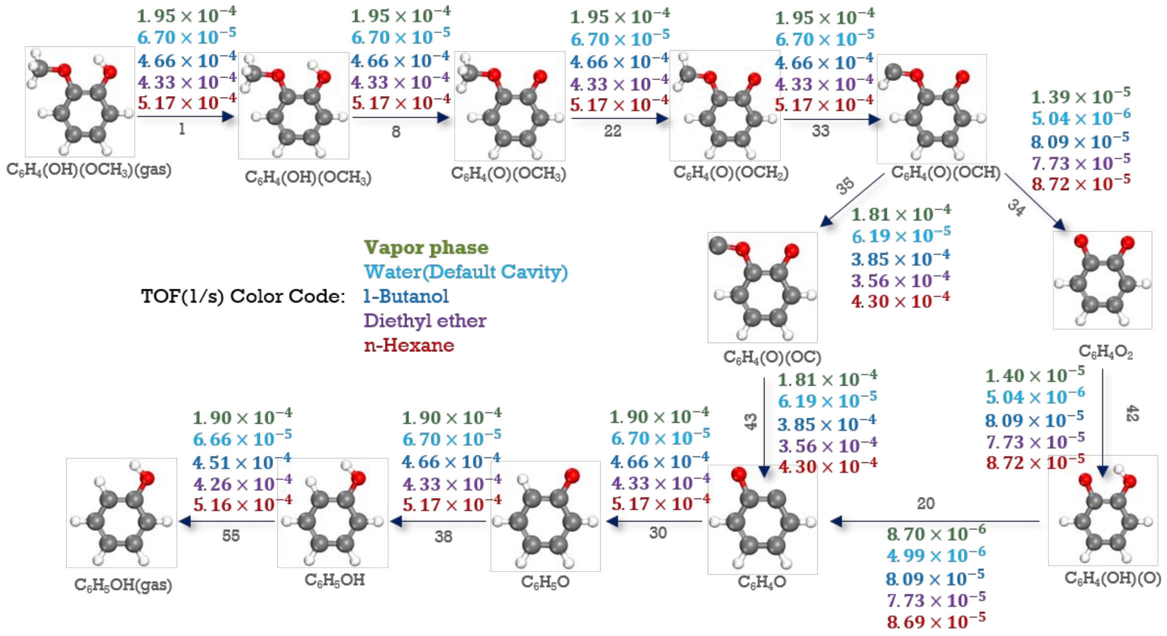

Figure 2: Turnover frequencies (1/s) along the dominant reaction pathway for the HDO of guaiacol to aromatic products over a Ru(0001) surface computed in different reaction environments.

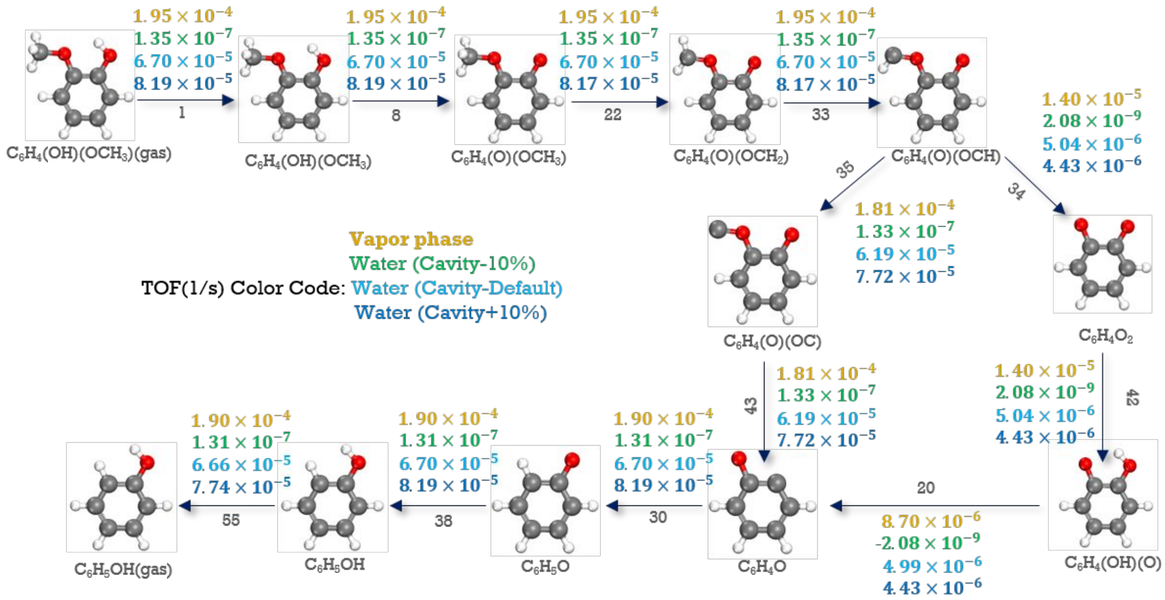

Figure 3: Turnover frequencies (1/s) along the dominant reaction pathway for the HDO of guaiacol to aromatic products over a Ru(0001) surface in vapor and aqueous phases. Aqueous phase calculations have been performed using three different cavity radius of Ru atoms.

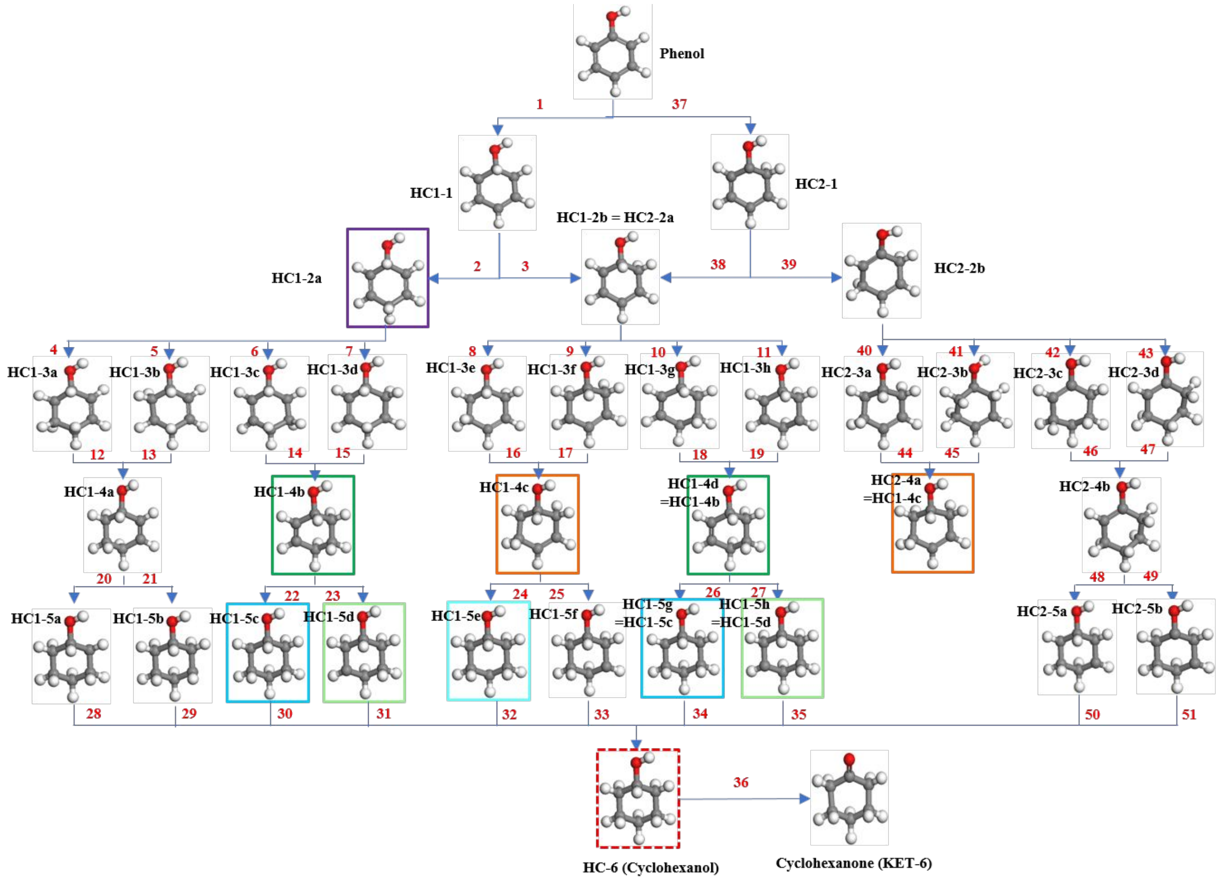

Figure 4: Reaction network investigated along the C_1 and C_2 hydrogenation pathway of phenol over a Ru(0001) model surface. Duplicate structures have been highlighted by identical border colors.

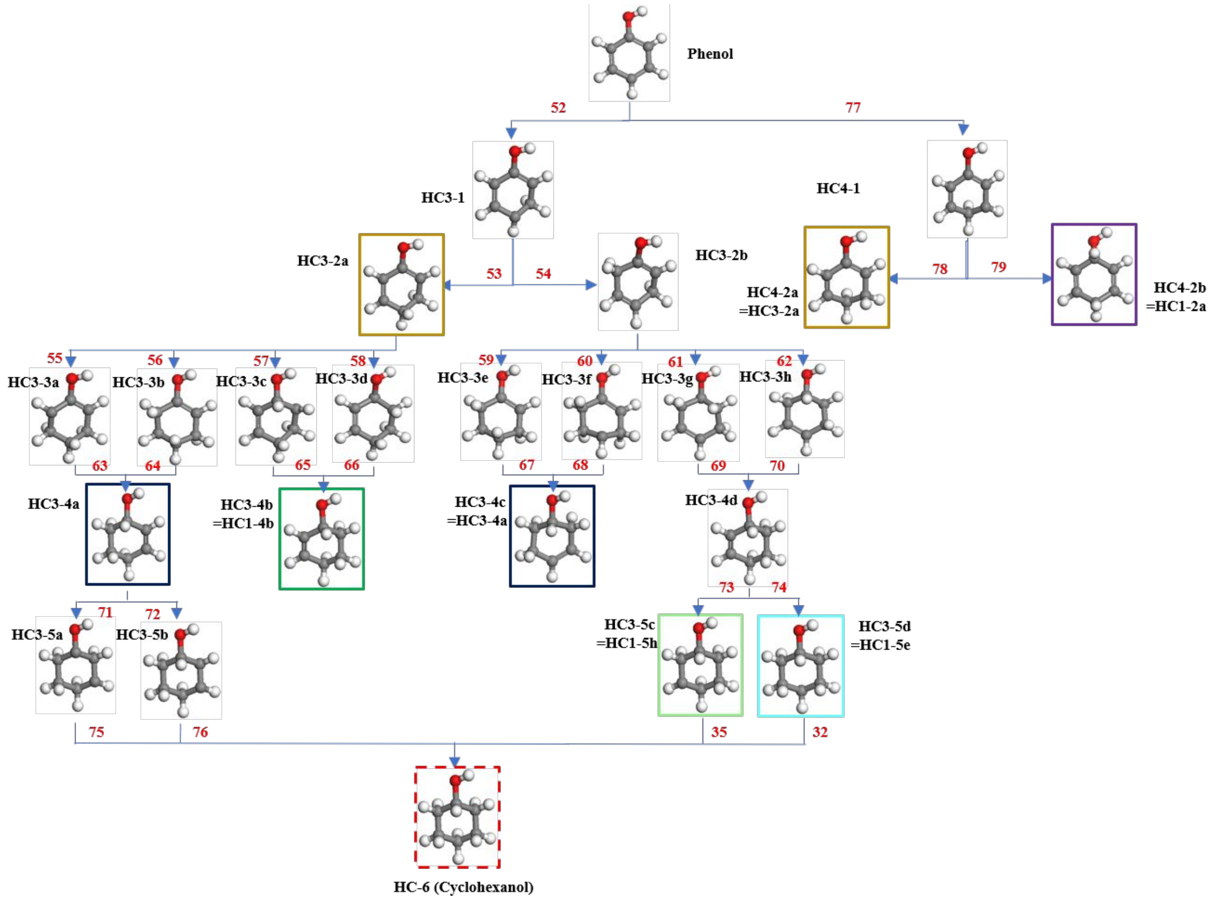

Figure 5: Reaction network investigated along the C_3 and C_4 hydrogenation pathway of phenol over a Ru(0001) model surface. Duplicate structures have been highlighted by identical border colors.

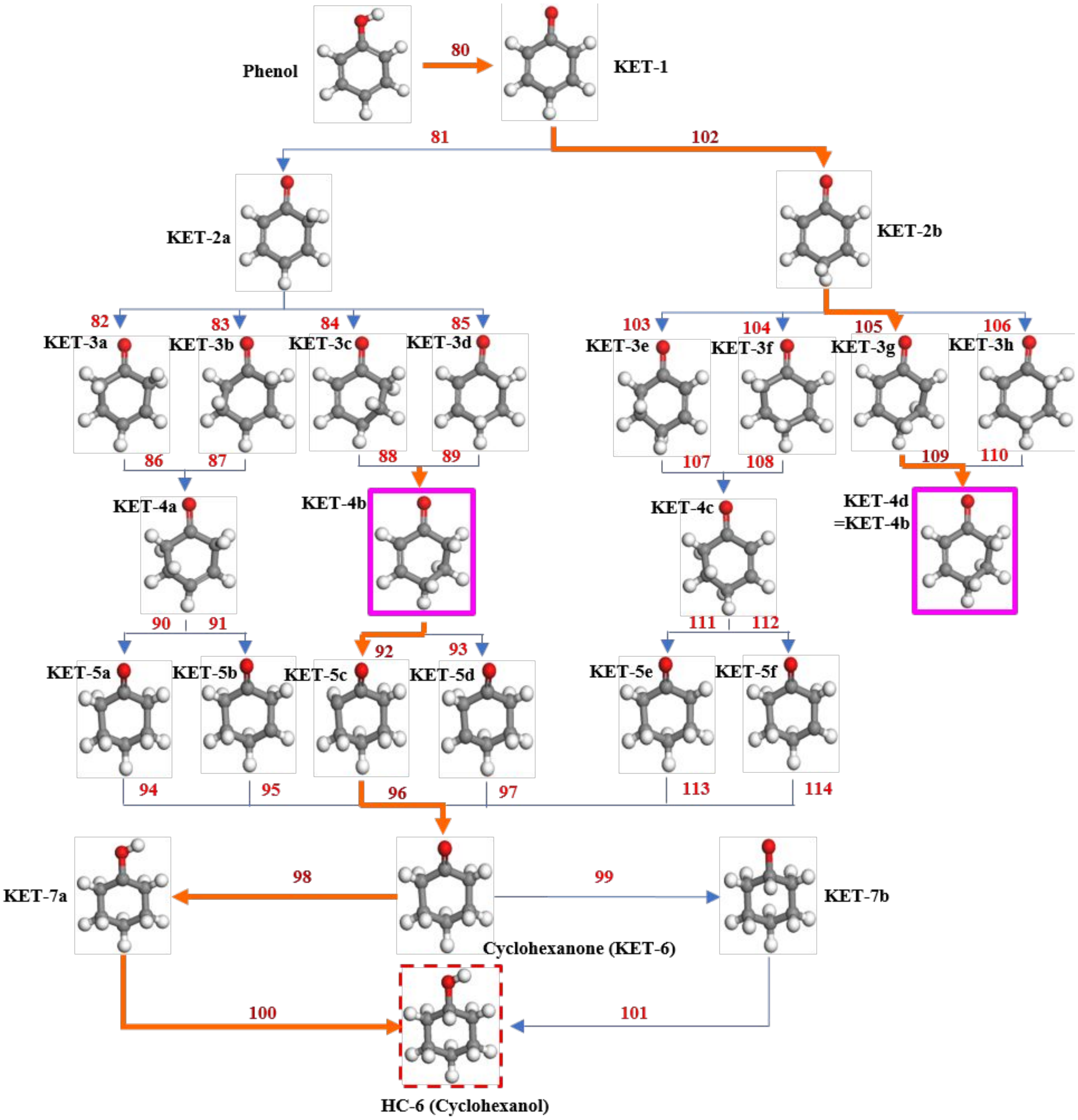

Figure 6: Reaction network investigated along the keto-enol tautomerization pathway of phenol over a Ru(0001) model surface. Duplicate structures have been highlighted by identical border colors. Proposed reaction mechanism and the reaction steps involved in the cycloalkane production from phenol have also been highlighted.

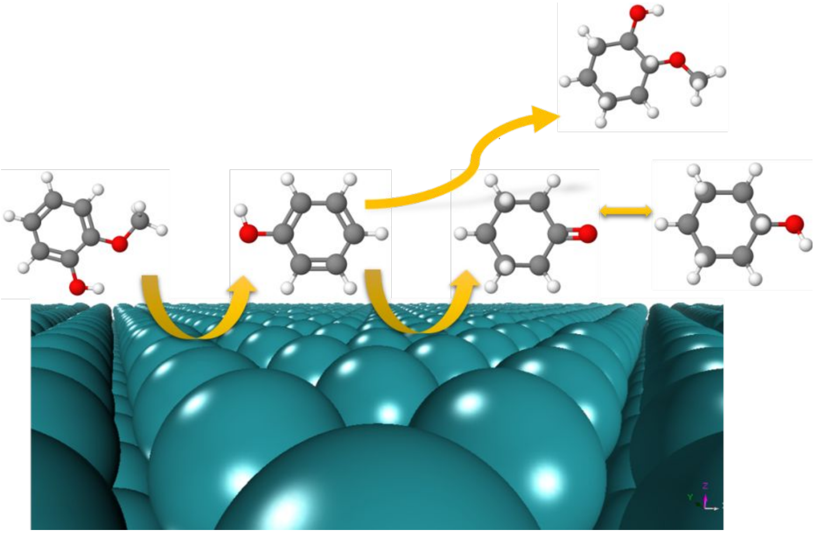

TOC